CONTROLLABLE GROWTH OF TELLURIUM-BASED FILMS BY ELECTROCHEMICAL DEPOSITION TECHNIQUE

YANG FAN

FACULTY OF ENGINEERING

UNIVERSITY OF MALAYA

KUALA LUMPUR

2023

CONTROLLABLE GROWTH OF TELLURIUM-BASED FILMS BY ELECTROCHEMICAL DEPOSITION TECHNIQUE

YANG FAN

RESEARCH REPORT SUBMITTED
IN FULFILMENT OF THE REQUIREMENTS FOR THE DEGREE OF
MASTER OF ENGINEERING SCIENCE

FACULTY OF ENGINEERING
UIVERSITI MALAYA
KUALA LUMPUR

2023

UNIVERSITY OF MALAYA

ORIGINAL LITERARY WORK DECLARATION

Name of Candidate: **Yang Fan**

Registration/Matric No: **17097341/2**

Name of Degree: **Master of Engineering Science**

Title of Project Paper/Research Report/Dissertation/Thesis ("this Work"):
CONTROLLABLE GROWTH OF TELLURIUM-BASED FILMS BY ELECTROCHEMICAL DEPOSITION TECHNIQUE

Field of Study: Advanced Materials/Nanomaterials (Materials Engineering)

I do solemnly and sincerely declare that:

(1) I am the sole author/writer of this Work;
(2) This Work is original;
(3) Any use of any work in which copyright exists was done by way of fair dealing and for permitted purposes and any excerpt or extract from, or reference to or reproduction of any copyright work has been disclosed expressly and sufficiently and the title of the Work and its authorship have been acknowledged in this Work;
(4) I do not have any actual knowledge nor do I ought reasonably to know that the making of this work constitutes an infringement of any copyright work;
(5) I hereby assign all and every rights in the copyright to this Work to the University of Malaya ("UM"), who henceforth shall be owner of the copyright in this Work and that any reproduction or use in any form or by any means whatsoever is prohibited without the written consent of UM having been first had and obtained;
(6) I am fully aware that if in the course of making this Work I have infringed any copyright whether intentionally or otherwise, I may be subject to legal action or any other action as may be determined by UM.

Candidate's Signature Date: 28th November 2023

Subscribed and solemnly declared before,

Witness's Signature Date:

Name:

Designation:

CONTROLLABLE GROWTH OF TELLURIUM-BASED FILMS BY ELECTROCHEMICAL DEPOSITION TECHNIQUE

ABSTRACT

Thermoelectric devices are composed of n-type and p-type materials. The purpose of this research was to study the controllability of tellurium (p-type) thin films. As for thin films, although the films are fabricated via many techniques, electrochemical deposition as one of many methods has some advantages, which can accurately control deposition parameters to obtain the corresponding film morphology and grain size. On the premise of being a material for thermoelectric microdevices, this work is aimed at growing a dense and homogeneous tellurium film in an atmospheric environment by electrodeposition at 300K. This study found that the CV curve shifts in the positive direction with increasing deposition time. Based on the findings, we set up the initial potential and the stabilized potential to study the tellurium film. In addition, three different additives (tartaric acid, polyvinyl alcohol, and sodium lignosulfonate) have been used and the pH was adjusted to optimize the morphology of tellurium films.

Keywords: Tellurium, Electrodeposition, Additives, Optimal morphology

PERTUMBUHAN FILEM BERASASKAN TELURIUM YANG TERKAWAL OLEH TEKNIK PEMENDAPAN ELEKTROKIMIA

ABSTRAK

Peranti termoelektrik terdiri daripada bahan jenis-n dan jenis-p. Tujuan penyelidikan ini adalah untuk mengkaji kebolehkawalan pembuatan filem nipis tellurium (jenis-p). Bagi filem nipis, walaupun filem dibuat melalui pelbagai teknik, pemendapan elektrokimia sebagai salah satu daripada banyak kaedah mempunyai beberapa kelebihan, antaranya boleh mengawal parameter pemendapan dengan tepat untuk mendapatkan morfologi filem dan saiz butiran yang sepadan. Atas premis sebagai bahan untuk peranti mikro termoelektrik, kerja ini bertujuan untuk menghasilkan filem tellurium yang padat dan homogen dalam persekitaran atmosfera melalui elektrodeposisi pada 300K. Kajian ini mendapati bahawa keluk CV beralih ke arah positif dengan peningkatan masa pemendapan. Berdasarkan penemuan, kami menetapkan potensi voltan awal dan potensi voltan stabil untuk mengkaji filem telurium. Di samping itu, tiga bahan tambahan yang berbeza (asid tartarik, polivinil alkohol, dan natrium lignosulfonat) telah digunakan dan pH telah diselaraskan untuk mengoptimumkan morfologi filem tellurium.

Kata kunci: Tellurium, pemendapan eletrokimia, bahan tambahan, pengoptimuman morfologi

ACKNOWLEDGEMENTS

I express my sincere gratitude to the University of Malaya for providing me with the esteemed opportunity to pursue postgraduate studies in science. Furthermore, I extend my heartfelt appreciation to the joint training program at the University of Chinese Academy of Sciences for offering me a conducive research environment. The knowledge and skills I have acquired through these institutions have been invaluable in furthering my academic and professional pursuits.

Dr. Mohd Faizul Mohd Sabri's guidance and assistance proved to be invaluable during the research process and in the field. Dr. Shaifulazuar Bin Rozali provided me with essential academic and time management advice, which played a vital role in my success. It was under his mentorship that I was able to develop a positive attitude and an aptitude for meeting deadlines. Dr. Nik Nazri Nik Ghazali, too, was a great source of encouragement and affirmation, and his support was a significant factor in my achievement. All three supervisors from UM demonstrated exceptional professionalism and expertise, and their contributions were instrumental in my academic growth and success.

Dr. Huaizhou Zhao allowed me to be jointly trained at the Chinese Academy of Sciences and taught me hard work and a serious attitude, Guodong Li paid attention to the experimental progress and discussed and analyzed the problems with me. Thanks to colleagues showed me the experimental equipment, tested samples, and recycled raw materials.

TABLE OF CONTENT

LIST OF FIGURES

LIST OF TABLES

LIST OF ABBREVIATIONS

Au	Gold
Bi-Te / Bi_2Te_3	Bismuth telluride
CA	Chronoamperometry
CE	Counter electrode
C_2H_6O	Anhydrous/absolute ethanol
C_3H_8O	Isopropanol
CV	Cyclic voltammetry
CVD	Chemical vapor deposition
CVT	Chemical vapor transport
Cu	Copper
DI	Deionized water
DEG	Diethylene glycol
EBD	Electron beam deposition
ECD	Electrochemical deposition
EG	Ethylene glycol
FESEM	Field emission scanning electron microscopy
FTO	Fluorine-doped tin oxide
FTEG	Flexible thermoelectric generator
GDR	Galvanic displacement reaction
HH	Hydrazine hydrate
H_2O_2	Hydrogen peroxide
HNO_3	Nitric acid

H_2S	Hydrogen sulfide
H_2SO_4	Sulfuric acid
KCl	Potassium chloride
LPE	Liquid phase epitaxy
MBE	Molecular beam epitaxial
$NaNO_3$	Sodium nitrate
$NaNbO_3$	Sodium niobate
NaOH	Sodium hydroxide
Ni	Nickel
NO_2	Nitrogen
NPs	Nanoparticles
NRs	Nanorods
NWs	Nanowires
OCV	Open circuit voltage
PC-Te	PEDOT: PSS coated Te
PEDOT	Poly(3,4-ethylenedioxythiophene)
PEDOT: PSS	Poly(3,4-ethylenedioxythiophene) polystyrene sulfonate
PF	Power factor
Pt	Platinum
PVA	Polyvinyl alcohol
PVD	Physical vapor deposition
PVDF	Polyvinylidene fluoride
RE	Reference electrode

RGO	Reduced graphene oxide
S	Seebeck coefficient
SA	Saturable absorber
Sb_2Te_3	Antimony telluride
SEM	Scanning Electron Microscope
Si	Silicon
Si_3N_4	Silicon nitride
SLS	Sodium lignosulfonate
SWCNT	Single-walled carbon nanotube
T	Absolute temperature
TA	Tartaric acid
TDEC	Diethyldithiocarbamate
Te	Tellurium
TEG	Thermoelectric generator
TeO_2	Tellurium dioxide
UV	Ultraviolet
WE	Working electrode
XPS	X-ray photoelectron spectroscopy
XRD	X-ray diffraction
ZT	Figure of merit
1/2/3-D	One/Two/Three-dimensional
σ	Electrical conductivity
κ	Total thermal conductivity

CHAPTER 1: INTRODUCTION

1.1 Overview

Thermoelectricity was first mentioned and researched in the mid-twentieth century as a new method to solve excess energy waste heat. The temperature difference between the cold and hot ends of a thermoelectric device generates electric power, which is widely used in refrigeration and power generation in the 21st century. Thermoelectric materials were employed in the area of microelectronic fields (Li et al., 2018), sensors (Wang et al., 2022), refrigerators (Chen et al., 2022), air conditioning (Bakthavatchalam et al., 2022), transportation (Vale et al., 2017), aerospace (Janak et al., 2015).

As for thermoelectric materials, the efficiency of TE material is governed by the figure of merit (ZT), which is defined as: $ZT = S^2\sigma T/\kappa$, where S is the Seebeck coefficient, σ is the electrical conductivity, T is the absolute temperature and κ is the total thermal conductivity of the materials. The ZT value has increased from less than 1 in 2010 to nearly 2.0 in 2020 with the deepening research. (El-Makaty et al., 2021) The high ZT value guarantees the quality of materials and devices.

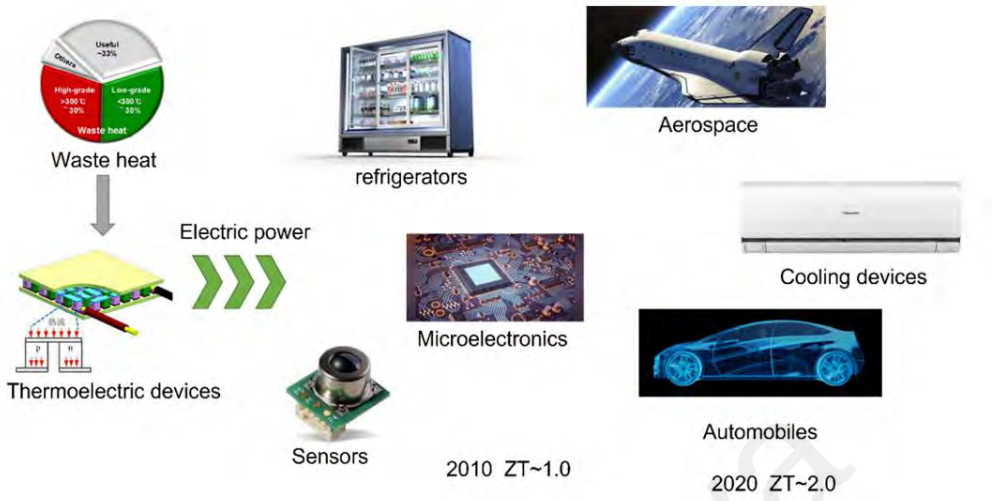

Figure 1.1 Development and application of thermoelectricity (Ref. El-Makaty et al. 2021)

The quality of thin film materials is one of the important indicators for high-quality chip production. Up to date, many technologies are used to fabricate a variety of thin films for chips, such as molecular beam epitaxial (Kang et al., 2019) (MBE), chemical vapor deposition (Newbrook et al., 2020) (CVD), thermal evaporation (Hamdi-Mohammadabad et al., 2022), electron beam deposition (Sudarshan et al., 2020) (EBD), sputtering (Zheng et al., 2014), and electrochemical deposition (Manoharan et al., 2021) (ECD). The films with different morphologies and properties are applied to devices and applications. However, deposition techniques have difficulties in some fields, such as controlling morphology, enhancing properties, and efficiently producing thin films. Based on these problems, we chose the technique of electrochemical deposition (ECD) to try to solve the deposition problem of p-type semiconductor tellurium and n-type semiconductor thin films, because of its advantages of efficient control of parameters and simple experimental conditions.

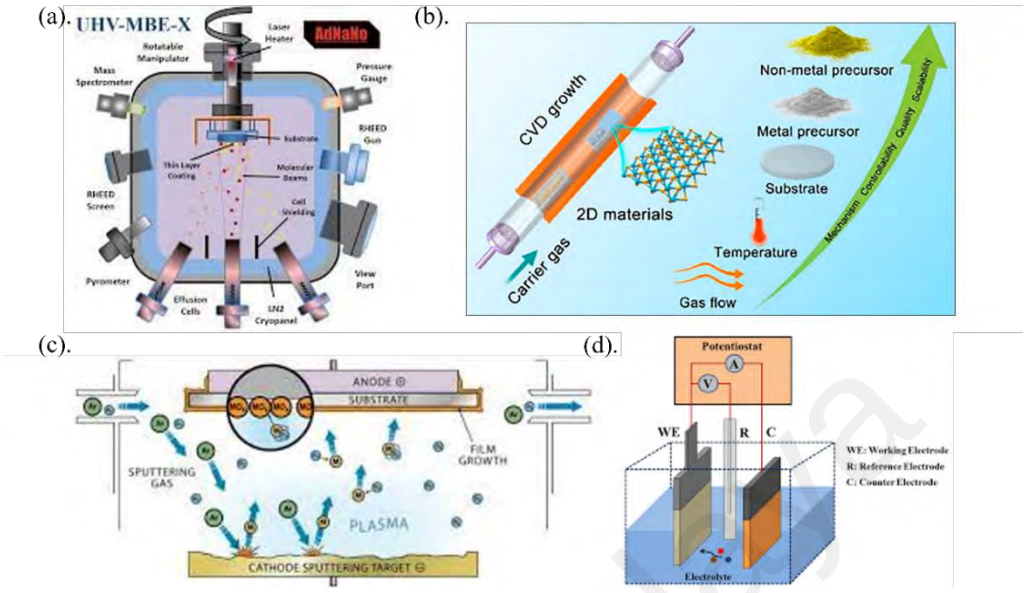

Figure 1.2 Schematic of technique (a) Molecular beam epitaxial (Ref. AdNaNo-tek) (b) Chemical vapor deposition (Ref. Tang et al., 2021) (c) Sputtering (Ref. Davidsbn, 2015) (d) Electrodeposition (Ref. Vanalakar et al., 2018)

1.2 Background

Tellurium is a novel semiconductor material. Since the 20th century, there have been many researchers studying tellurium thin films or tellurium doping creating different structures to suit different application fields via different techniques, such as galvanic displacement (Rheem et al., 2010), thermal vacuum evaporation (Tsiulyanu et al., 2013), typical chemical (Choi et al., 2014), electrochemical technique (Abad et al., 2015), non-hydrolytic sol-gel process (Shen et al., 2016), solvothermal method (Li et al., 2017), vacuum-assisted filtration (Song et al., 2017), hydrothermal method (Wang et al., 2018), Low-temperature chemical reduction approach (Tsao et al., 2019) water-based scalable synthetic method (Karalis et al., 2021), physical vapor deposition (PVD) (Yang et al., 2021), wet

chemical assisted synthesis (Saxena et al., 2021), chemical vapor transport (CVT) (Zhao et al., 2022).

Tellurium, a narrow bandgap p-type semiconducting TE material, it has deserved wide attention because of its thermoelectric, photoconductive, piezoelectric, and optical properties. Low-dimensional Te-based nanomaterials show unique internal features, an elemental electrical switch was designed via phase-change memory (Shen et al., 2021). Apte et al. (2021) reported that two-dimensional α-Tellurium films have great piezo-response (piezoelectric coefficient 1pm/V). In addition, Raman spectroscopy under strain and magneto-transport has been shown by one-dimensional van der Waal material Tellurium and recorded by Du et al. (2017). Table 1.1 shows the different types of tellurium materials and their performance.

Table 1.1 Various types of tellurium and their various properties

Tellurium (types)	Year(s)	Properties	Reference
Films with SLS	2015	Seebeck 285μV/K PF 280μW/mK^2	B. Abad et al.
Cu-doped	2020	Seebeck -227μV/K PF 5.6mW/mK^2	S. Lal et.al
Nanowire	2018	Seebeck 551μV/K Conductivity 1.29 S m^{-1}	W. Wang et al.
α-Tellurene films	2020	Piezoelectric coefficient (d_{33}) 1 pm/V	A. Apte et.al
Te/PMMA grains	2018	Absorbance was constant in 310-2200nm, the photocurrent increases linearly as the optical power density	U. Coscia et al.
Nanowire	2016	Absorb the UV light and visible Resistivity range from 48.8 ± 0.4×10^{-2} to 13.2 ± 0.8×10^{-2} Ω·m	N. Kumar et al.

Tellurium plays an important role as the main component or as a dopant. Lai et al. (2020) studied the enhancement of properties of thermoelectric Te films doped with Cu at different concentrations. Xin Bo et al. (2019) and Lim et al. (2009)

investigated Sb_2Te_3 in thermoelectric film fields. The morphology of Bi-Te alloy nanoparticles synthesized via electrodeposition was analyzed by Gan et al. (2010). Indium and tellurium co-doped bismuth selenide single crystals have been produced by melt growth technique by Hegde et al. (2021). Rudnik et al. (2013) used an electrochemical technique to study co-deposition of copper and tellurium. Tellurium copper compounds exhibit polycrystalline p-type semiconductors behavior.

1.3 Problem statement

Nowadays, film products are fabricated through different technologies and applied in various fields. Different film morphologies are required for applications with different properties. A systematic prediction is possible for the growth of various types of thin films, such as photocatalytic film (Cabrera et al., 2012), photo-response nanorods (Kang et al., 2019), photoelectrochemical films (Mohsen Momeni & Najafi, 2021), piezo-response films (Apte et al., 2021), piezoelectric film (Chuai et al., 2021), thermoelectric film (Van Toan et al., 2020). As for thermoelectric materials, the anisotropic structures have a huge impact on the characterization and properties of micro-thermoelectric devices. The dense thick films are favored in thermoelectric fields. Film morphology may affect material properties, thus, controlling the growth of the sample surface morphology is critical. Compared to other deposition methods, electrochemical deposition techniques have many advantages, which are fast sample deposition, sample purity and cost-effectiveness. It is necessary for easily adjusting the parameters to

control the sample morphology as much as possible during the experiment process. The study of growing films with specific morphologies is valuable. Glatz et al. (2008) reported the thick layers of $Bi_{2+x}Te_{3-x}$ with controlled stoichiometry. Xin Bo et al. (2019) have researched on controllable electrochemistry and its mechanism. The mechanism of underpotential deposition is proposed by Santos et al. (2011). Electrodeposition method can easily control these parameters (potential, current, electrolyte concentration and deposition time) to achieve the mastery of thin film morphology.

Most studies pay attention to the properties, with less discussion on morphology. As for films in the thermoelectric field, dense and thick morphology is critical. This study selected the optimized potential (stable potential) by CV curves and additives to improve the tellurium film morphology. The morphology of sample is indeed more optimized with stable potential, polyvinyl alcohol (PVA) additives (stable potential) and sodium lignosulfonate (SLS) additives (stable potential). Tellurium films are more homogeneous, reaching a thickness of 1-2μm.

1.4 Objectives of the study

The objectives of the study are as follows:

1. To preliminary explore the electrodeposition of tellurium film by comparing the chronoamperometry and fast pulse deposition methods.

2. To study the Cyclic Voltammetry curve of tellurium and find out the optimized potential to control fabrication of density and homogeneity thin films.

3. To improve tellurium morphologies by using surfactants/additives.

1.5 Scope of works

In this study, firstly the cyclic voltammetry curve of Te will be analyzed. Based on the CV curve, the morphology of the tellurium films fabricated at both stable and initial potential was studied and compared. The effects of additives and the pH value of electrolytes on the morphology of tellurium films will be investigated in detail. Optimization of the morphology of tellurium films will be carried out at the final stage of this study.

CHAPTER 2: LITERATURE REVIEW

2.1 Introduction

This section aims to provide an overview of the literature on tellurium and its applications in different fields as the main component and doping. In addition, not only the properties of tellurium will be introduced, some literatures on the morphologies of tellurium will be also covered in this section.

2.2 Modification of Tellurium

Tellurium has made many advances in some fields in the last ten years, such as the performance optimization of thermoelectric materials, thermoelectric devices, gas sensors, optical absorption, and its response. Improvising of thermoelectric materials has long been the focus of attention in the world.

In the fields of organic hybrid for tellurium materials, Choi et al. (2014) reported about their findings on tellurium nanowires (Te NWs) films hybridized with single-walled carbon nanotube (SWCNT) as a flexible thermoelectric material via the typical chemical procedure. The electrical conductivity and figure of merit (ZT) have significantly increased from 4 to 50 $S \cdot m^{-1}$ and 0.05×10^{-2} to 0.45×10^{-2}, respectively.

Abad et al. (2015) reported about thermoelectric properties of tellurium films with sodium lignosulfonate (SLS) additive prepared by electrochemical deposition. Its power factors reached maximum values of $415\,\mu W/m \cdot K^2$ without SLS and

110μW/m·K^2 with SLS at 105℃.

In the same year, Gao et al. prepared the water processable RGO/Te (reduced graphene oxide) nanowires (NWs) hybrid films. These hybrid films with maximum power factor (68.4μW/mK^2), electrical conductivity (633S·m^{-1}) and Seebeck coefficient (382 μV/K) have been enhanced better than before the modification.

In addition, Wang et al. (2018) synthesized ultra-fine Te NWs with a diameter of 10-35nm by a hydrothermal route. The Seebeck coefficient of Te NWs films was as high as 551μV/K and the thermal conductivity was as low as 0.16Wm^{-1}K^{-1}. Its electrical conductivity and ZT values were 1.29S·m^{-1} and 0.72×10^{-3} at room temperature. Te/PVDF (Te with polyvinylidene fluoride) films could be rolled up on a pencil to show good flexibility.

Liu et al. (2020) successfully prepared the $NaNbO_3$/Te-NRs (nanorods) composites via a hydrothermal method. The introduction of $NaNbO_3$ effectively improves the environmental stability of Te-NRs. The electrical conductivity and Seebeck coefficient of $NaNbO_3$/Te-NRs achieve increase simultaneously at room temperature, when the mass ratio of $NaNbO_3$:TeO_2 is 1:1, the highest PF value reach 43.5μWm^{-1}K^{-2} and ZT is achieved for 0.081.

Moreover, Ni et al. (2020) found that a unique free-standing flexible Te-coated PEDOT (Poly(3,4-ethylenedioxythiophene)) hybrid films could be prepared by electrodepositing Te nanostructures on PEDOT NW film. The hybrid films were optimized and achieved the maximum PF of 240.0 μW^{-1}K^{-2} and electrical conductivity of 561.4S·cm^{-1} at room temperature. The Seebeck coefficient was

65.4 μ VK^{-1}. Some researchers reported on TE performance of tellurium synthesized by different methods are shown in Table 2.1.

Table 2.1 Synthesis of Te materials via different methods and their Te properties.

Reference	Composition	Methods	Seebeck coefficient (μV/K)	Power factor ($\mu Wm^{-1}K^{-2}$)	ZT 10^{-2}
Choi et al. 2014	TeNWs/SWCNT	Typical chemical	-	3.87	0.45
Abad et al. 2015	Te/SLS	Electrochemical technique	285	110	3
Gao et al. 2015	RGO/TeNWs	Water-based synthetic	382	68.4	-
Wang et al. 2018	Ultra-fine TeNWs	Hydrothermal	551		0.072
Liu et al. 2020	$NaNbO_3$/TeNRs	Hydrothermal		43.5	8.1
Ni et al. 2020	TeNWs/PEDOT	Electrochemical technique	65.4	240	

As for TE devices, a thermoelectric film device was produced by Li et al. (2017). Bi_2Te_3 nanowires (NWs) as n-type leg and Te-PEDOT:PSS (Poly(3,4-ethylenedioxythiophene) polystyrene sulfonate) as p-type leg. This film has shown a higher thermoelectric performance and better environmental stability. The thin-film device has a stable output voltage of 56mV and a high output power density value of 32μW·cm^{-2} at a temperature difference of 60K.

At the same time, Song et al. (2017) showed the fabrication of flexible PEDOT:PSS/PF-Te ((PEDOT:PSS) functionalized Te) nanorods by a vacuum-assisted filtration process for the 8 single-leg flexible thermoelectric generators to generate an output voltage of 2.5mV at a 13.4K temperature difference between the human body and the enviroment.

Single-walled carbon nanotube (SWCNT)/PEDOT:PSS coated Te nanorod (PC-Te) composite films were fabricated by a simple vacuum assisted filtration method by Meng et al. (2019). They were tested on pristine and H_2SO_4-treated composite films by XRD, SEM, FESEM (Field emission scanning electron microscopy), Raman spectra, XPS (X-ray photoelectron spectroscopy), and Temperature dependence. The open circuit voltage (OCV) and maximum output power were 5.6mV and 53.6nW, respectively, at a temperature difference of 44K.

In addition, a composite PEDOT:PSS/$PVA_{10\%}$/Te-$NWs_{35\%}$ fiber was prepared and showed the best thermoelectric and mechanical properties, which had enhanced the electrical conductivity of 382.4S·cm^{-1} and power factor of 8.5μW/mK^2 by the ethylene glycol (EG) post processing. The as-fabricated fiber-based thermoelectric generator (FTEG) with ten legs of EG-PEDOT:PSS/$PVA_{10\%}$/Te-$NWs_{35\%}$ showed an acceptable output voltage of 5.03mV and power density of 28.87μW cm^{-2} at a temperature difference of 60K (Yang et al., 2021).

At the same time, PEDOT:PSS/tellurium nanowires organic/inorganic hybrid fibers were fabricated for flexible TE generator without substrates by Liu et al. (2021). A high power factor of 17.8μW/mK^2 was achieved for H_2SO_4 post-treated PEDOT:PSS/Te-NWs hybrid fiber with 50wt% Te-Nws, as a simple flexible TE generator of post-treated hybrid fibers with six pairs of p-n fiber legs.

Additionally, a PEDOT:PSS/Te double-layer structured thin firm devices can greatly increase the conductivity up to 10^{-6}S·cm^{-1} and improve the Seebeck coefficient from 12μV/K to 650μV/K. Among other results, the Fermi level of the PEDOT:PSS/Te interface approaches the conduction band with increasing

temperature, thereby increasing the effective carrier concentration (Liang et al., 2021). Table 2.2 shows the TE properties and applications of Te.

Table 2.2 Synthesis of Te materials, different routes, properties and their applications

Reference	Composition	Methods	Seebeck coefficient (μV/K)	Power factor ($\mu Wm^{-1}K^{-2}$)	Content/ Application
Li et al. 2017	Te-PEDOT:PSS	Solvothermal	477	4.5	TE film devices
Song et al. 2017	PEDOT:PSS /PF-Te	Vacuum-assisted filtration	151	51.6	8 single-leg flexible TE generator
Meng et al. 2019	SWCNT:PEDOT :PSS/PC-Te	Vacuum assisted filtration	56	104	Enhanced properties /TE generator
Liang et al. 2021	PEDOT:PSS/Te film	Water-based synthetic	650	-	Thin-film devices
Karalis et al. 2021	PEDOT:PSS/Te NWs	Water-based synthetic	383.2	102.42	Thermoelectric generator (TEG)
Yang et al. 2021	PEDOT:PSS, PVA/Te NWs	Gelation	18	8.5	Flexible/wearable fiber-based TEG
Liu et al. 2021	PEDOT:PSS/Te NWs	Hydrothermal	25.5	17.8	Flexible fiber-TEG

Several breakthroughs in the field of tellurium research have been reported on the optimization of thermoelectric properties and the fabrication of thermoelectric devices such as tellurium nanowires (Te NWs), nanorods (Te NRs) nanoparticle (Te NPs) and single crystals.

Rheem et al. (2010) reported that one-dimensional (1D) nanostructures were found to decrease thermal conductivity via phonon scattering. They demonstrated for the first time the synthesis of Te nanotubes with controlled diameter (10nm) and wall thickness (15-30nm) from sacrificial Co nanowires (NWs) by galvanic displacement reaction (GDR) at room temperature.

In the same year, the uniform Te nanoflakes (2D) were synthesized at 440℃ and d ≈ 490nm via pyrolyzing a single-source molecular precursor diethyldithiocarbamates tellurium (TDEC) by Wang et al. (2010). Their team

realized TDEC film with the thickness of 490nm, 6.4 μm and 13.8 μm, respectively.

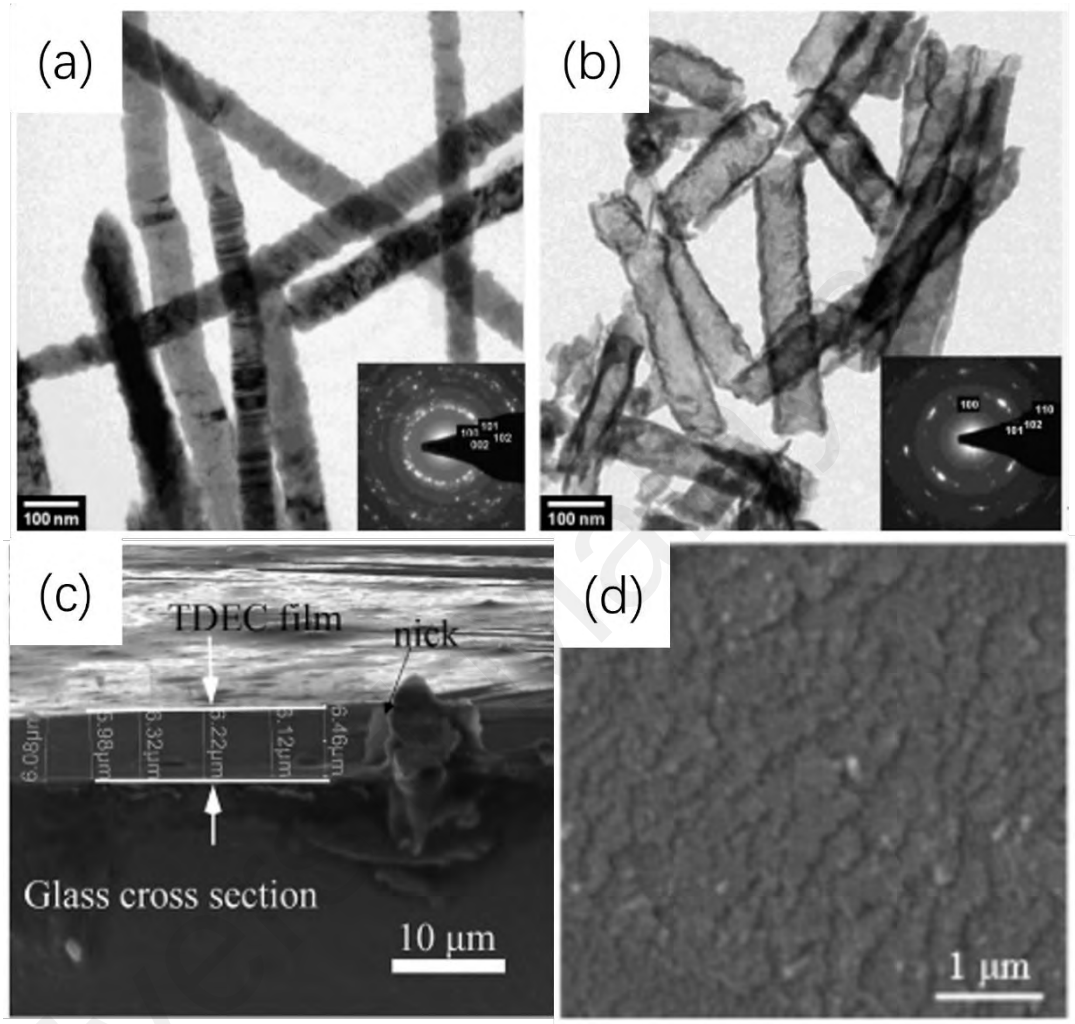

Figure 2.1 TEM images and selected area electron diffraction pattern of (a) electrodeposited cobalt nanowires and (b) tellurium nanotube (Ref. Rheem et al., 2010) SEM images of the Te films prepared by pyrolysis of 6.4 μm TDEC films (c) cross-section (d) surface (Ref. Wang et al., 2010)

In the fields of tellurium nanomaterials, Wu et al. (2014) comprehensively demonstrated Te heterostructures, including 1-D (nanowires) and 3-D (branched nanorods), synthesized by galvanic displacement reaction using zinc foils as sacrificial materials in alkaline baths. Te nanowires (Te NWs) were fabricated from 4 to 50℃, showing increasing diameters from 49nm to 200nm. The branched

nanostructures and glass-like morphology appeared in the surface.

Ge et al. (2017) successfully grow single-crystalline Te microtube and rods, by controlling NaOH content using a hydrothermal reduction method.

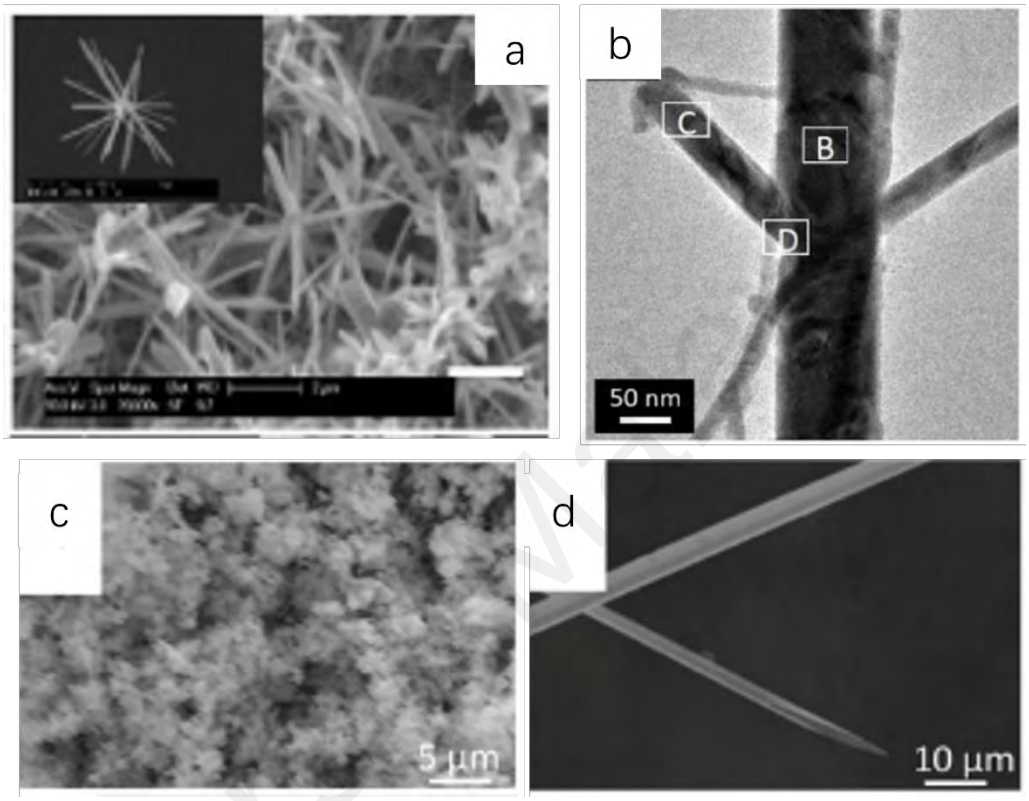

Figure 2.2 Images of the Te branched nanostructures synthesized at 10 mM with a fixed pH of 13.1 at 23℃ (a) SEM (b) TEM (Ref. Wu et al., 2014) SEM images of Te powders after hydrothermal reaction with 0.5g NaOH (c) Te microtubes obtained with 1g NaOH (d) (Ref. Ge et al., 2017)

It is worth mentioning that Saxena et al. (2021) found a new route to synthesize the Te nanoparticles (Te NPs) rapidly. The hexagonal phase of Te crystal grains was observed. This approach prepared the Te NPs by wet chemical method using DEG (Diethylene glycol) and HH (Hydrazine hydrate) in 10 min without templates, surfactants, high temperature and pressure for reaction.

The latest research showed that Te nanoflakes with high quality was synthesis in one step via chemical vapor transport (CVT). By adjusting the temperature to tune

the growth kinetics, Te nanoflakes with a lateral size of 45μm and a thickness of approximately 70 nm can be obtained. The fabricated 2D Te nanoflakes showed excellent electrical properties and a high mobility of 379cm^2 V^{-1} s^{-1}. (Zhao et al., 2022) Specific details of low dimensional structure were summarized in Table 2.3.

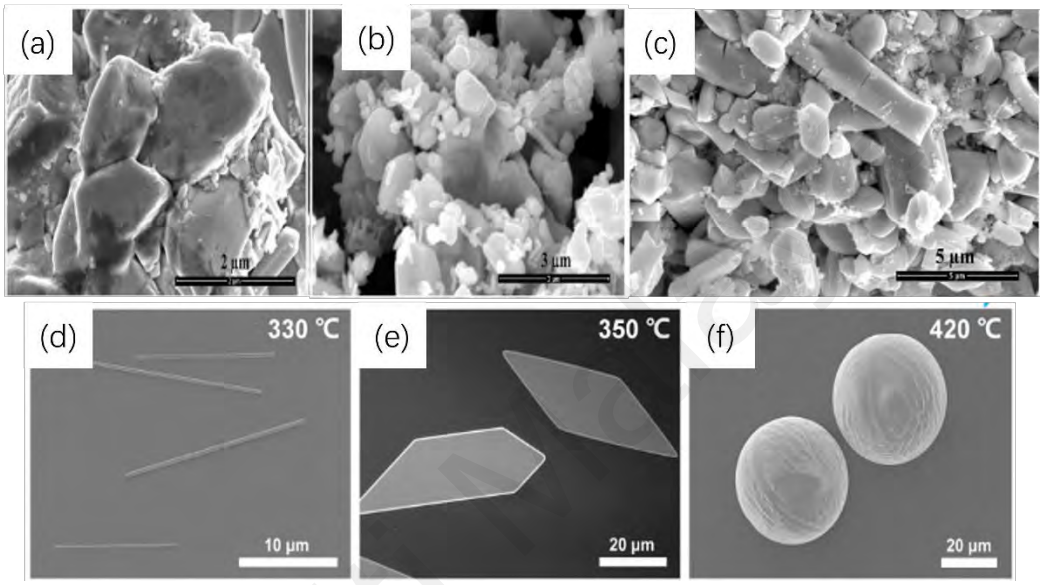

Figure 2.3 FESEM image of Te nanoparticles with solvents (a) Te powder + HH + DEG (b) Te powder + HH + DEG + 120℃ (c) K_2TeO_3 + HH + DEG + 120℃ (Ref. Saxena et al., 2021) SEM image of Te with different morphologies were obtained at (D) 330℃, (E) 350℃, and (F) 420℃ (Ref. Zhao et al., 2022)

Table 2.3 Morphology of 1-3D Te nanostructure by different methods.

Reference	Low dimensional structure	Methods	Properties
Rheem et al. 2010	1D Te nanowire	Galvanic displacement	Low mobility Grain size of 10nm
Wang et al. 2010	2D Te nanofilm	Pyrolyzing	Uniform nanoflakes d≈490nm
Wu et al. 2014	1D Te nanowires 3D branched nanorods	Galvanic displacement	Single crystalline Diameters of 49-200nm
Ge et al. 2017	Te micro tubes/rods	Hydrothermal reduction	Single crystalline 10-50μm in diameter
Saxena et al. 2021	Te nanoparticles	Wet chemical assisted synthesis	Rapid synthesis without harsh conditions
Zhao et al. 2022	2D Te nanoflakes	Chemical vapor transport	Controllable synthesis of films 45 mm lateral and 70 nm thickness

In recent years, some progress has been made in tellurium practical applications, together with continuous efforts of researchers in the development and exploration of tellurium materials. Gas sensors, optical absorption, wearable devices, and fiber thermoelectric generators were fabricated and received high attention. Even some aspects of potential applications have been compared with conventional aspects, which will begin to pass into the production stage. Several application scenarios are introduced in the following Figure 2.4.

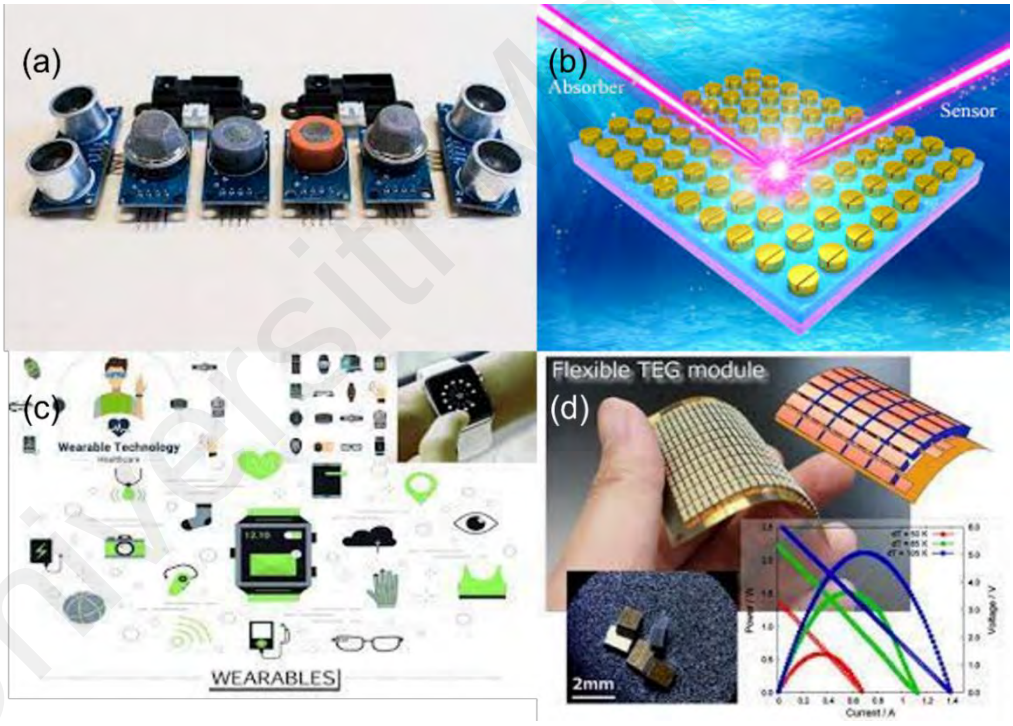

Figure 2.4 Potential applications for tellurium materials (a) gas sensor (Ref. Apogeeweb, 2021) (b) optical absorber (Ref. Liu et al., Guest Editors) (c) wearable device (Ref. Fahad, 2020) (d) flexible thermoelectric generators (FTEG) (Ref. Sugahara et al., 2019)

In the decade of literature review for potential application, especially, in the field of gas sensors, Tsiulyanu et al. (2013) demonstrated that the tellurium films prepared via thermal vacuum evaporation have shown high sensitivity to low

concentrations of NO_2 at room temperature with considerably short response time. The Te thin films have a thickness of 110nm and 30nm, and the surfaces of these films are smooth.

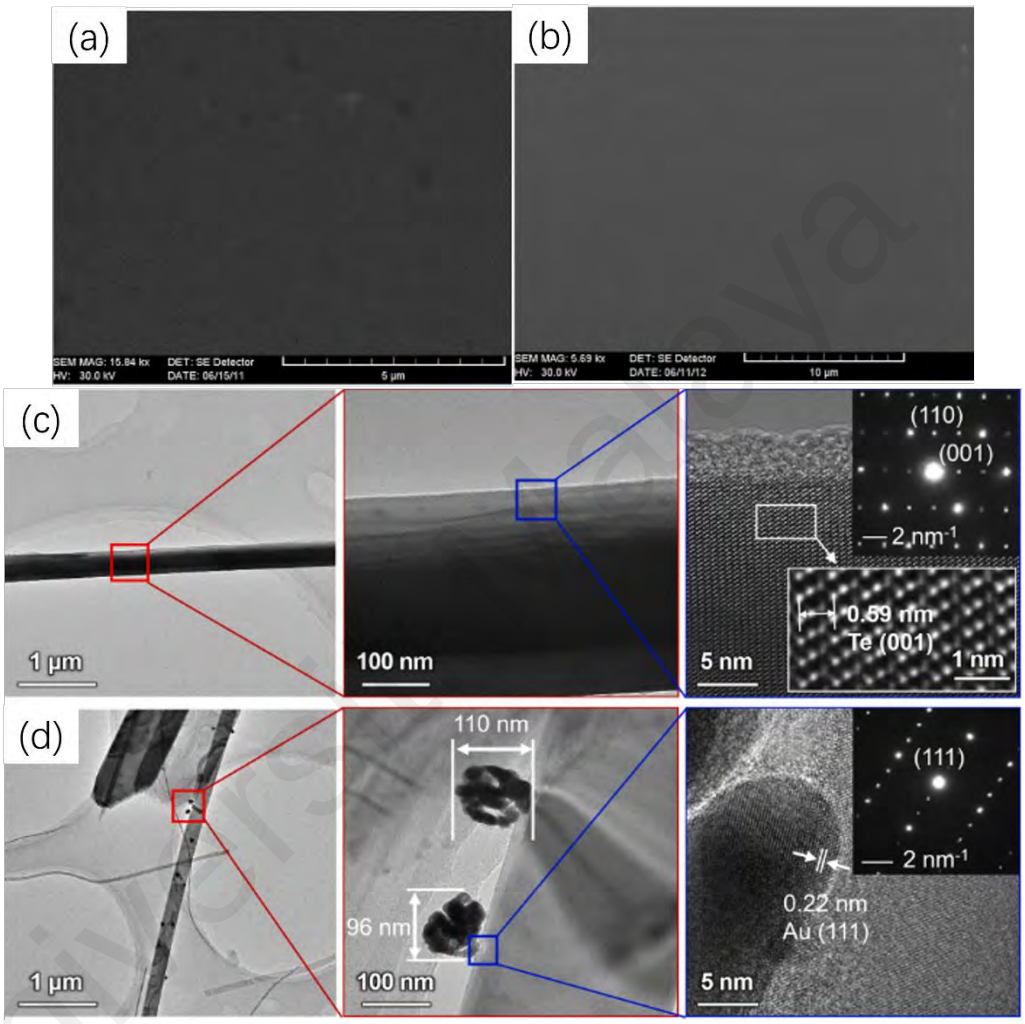

Figure 2.5 SEM images of Te (a) thin 110nm and (b) ultrathin 30nm (Ref. Tsiulyanu et al., 2013) TEM images of Te and Au@Te. (c) Te nanobelt (SAED pattern) (d) Au@Te (SAED pattern) (Ref. Yuan et al., 2022)

The latest research by Yuan et al. (2022) which successfully fabricated the 18nm Te nanobelts and flower-like Au nanoparticles with a diameter of 50–200nm synthesized through a one-pot hydrothermal process. Subsequently, they used the fabricated Au-Te materials to produce an Au@Te sensor, which shows sensitivity of $0.028ppb^{-1}$ (0–50ppb), a limit of detection with ppt-level (~83ppt), rapid

response (11.3s towards 5ppm), good repeatability and selectivity.

In addition, H_2O_2 sensor performance of Te nanoparticles (Te NPs) modified glassy carbon electrode exhibited high sensitivity of $0.83 mA \cdot mM^{-1} \cdot cm^{-2}$ with a correlation coefficient of 0.995 in the range of 0.67 to 8.04μM. Manikandan et al. (2017) reported that Te nanoparticles (Te NPs) synthesized by wet chemical method have a hexagonal phase with spherical morphology (307 nm).

Waldiya et al. (2019) proposed a novel non-enzymatic and low-cost sensor based on tellurium nanoparticles (Te NPs) for the analytical determination of H_2O_2. Te NPs/FTO (Fluorine-doped tin oxide) fabricated at applied potential of −1.40 V showed excellent electrocatalytic activity for H_2O_2 reduction and produced densely packed nanoparticles with high surface energy. The proposed Te NPs/FTO sensor shows an excellent sensitivity of $757 \mu A mM^{-1} cm^{-2}$. The sensor possesses good selectivity and stability with an excellent response time of about 5s in amperometry.

Moreover, TeO_2 thin films exhibited reversible and quick response to ethanol gas at range of 125-225℃ and ethanol concentration of 100-1000ppm. The peak response was 9.5 at 200℃ with the 1000ppm ethanol gas. Shen et al. (2016) synthesized Te thin films with tetragonal structures with a diameter of 80-350nm and a length of 250-900nm prepared by non-hydrolytic sol-gel process.

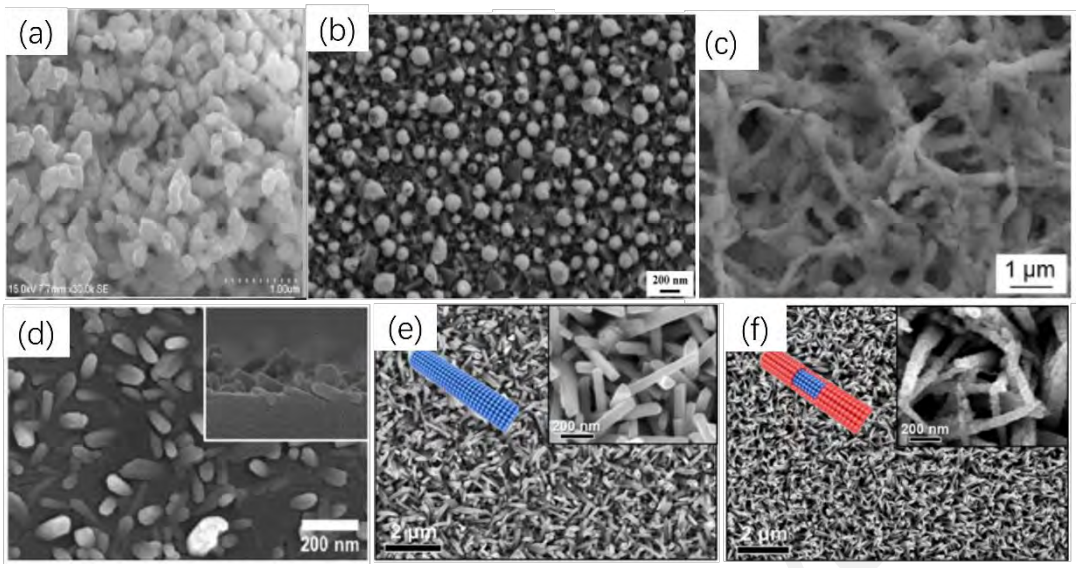

Figure 2.6 (a) SEM images of Te NPs synthesized by wet chemical method (Ref. Manikandan et al., 2017) (b) FESEM images of TeNPs electrochemically deposited at -1.30 V onto FTO substrate using [BMIM][Ac] at 90 °C (Ref. Waldiya et al., 2019) (c) High magnification FESEM image of TeO_2 thin films synthesized by non-hydrolytic sol-gel process (Ref. Shen et al., 2016) (d) FE-SEM images of rice-like Te thin films grown by galvanic displacement reaction on the Si wafer in 30 minutes. (Ref. Hwang et al., 2019) SEM images of Te NWs before (e) and after (f) the detection of 1μM Hg^{2+} ions (Ref. Tsao et al., 2019)

Additionally, a study on rice-like tellurium films using a galvanic displacement reaction (GDR) on a silicon wafer and their response to hydrogen sulfide (H_2S) gas at room temperature was conducted by Hwang et al. (2019) The rice-like Te films of 15-50nm was used as Te sensor materials which showed ultra-high sensing response to H_2S (~1000% at 100ppm of H_2S) an excellent response toward H_2S gas (ranging from 15ppb to 90ppm).

Not just in the gas sensing application, tellurium nanowires (Te NWs) could also as core material in thermoelectric nanosensor for the detection of mercury ions (Tsao et al., 2019). The Te NWs was growth by a low-temperature chemical reduction method. The device can provide high sensitivity (LOD of 1.7nM) and

good linear range (from 10nM to 1μM) of mercury ion detection. Tellurium nanowires with 1μM of mercury ion detected on the morphological surface are rougher than tellurium nanowires. In all, synthesis routes of Te materials and their application in the field of gas sensors are summarized in Table 2.4.

Table 2.4 Synthesis of tellurium materials via different routes applied in the field of sensor.

Reference	Materials	Methods	Content/Application
Tsiulyanu et al. 2013	Te films	Thermal vacuum evaporation	Concentration of NO_2 and gas sensitivity
Shen et al. 2016	TeO_2 films	Non-hydrolytic sol-gel process	Ethanol gas sensing with temperature
Manikandan et al. 2017	Te nanoparticles (Te NPs)	Wet chemical	The H_2O_2 sensor
Tsao et al. 2019	Te nanowires (Te NWs)	Low-temperature chemical reduction	Thermoelectric nanosensor of mercury (Hg^{2+}) ions
Hwang et al. 2019	Te films	Galvanic displacement	Ultra-high sensing response to H_2S gas
Waldiya et al. 2019	Te nanoparticles (Te NPs)	Electrochemical technique	The H_2O_2 sensor possess good selectivity and stability
Yuan et al. 2022	Au@Te nanobelts	One-pot hydrothermal	Au@Te sensor for NO_2 with good repeatability and selectivity

Not just the gas sensors, researchers have made significant progress in the study of tellurium thin films in photo response and saturable absorber (SA). Initially, The tellurium nanorods (Te NRs) were prepared by template and non-surfactant electrochemical technique from an aqueous solution at room temperature by Li et al. (2012), and the photo response test found out that tellurium nanorods (Te NRs) exhibited enhanced conductivity in illumination.

Coscia et al. (2018) reported that tellurium nanopowders with average size of 8.4$\pm$0.4nm were prepared by dry vibration milling technique followed by liquid phase sedimentation procedure. Its Photoconductivity measurements showed that responsivity is independent of the wavelength of the incident radiation and was

directly proportional to the optical absorbance.

In the same year, a group of researchers demonstrated that ultra-long feather-like Te film can be obtained at − 0.31V for 300s on Ni substrate by electrodeposition without agent (Mu et al., 2018). The results revealed feather-like Te films with a preferred (110) orientation, which have hexagonal structures and strong light absorption in the visible range. The conductivity and photocurrent were 20.63×10^{-5}S/cm and 0.0170mA/cm^2, respectively.

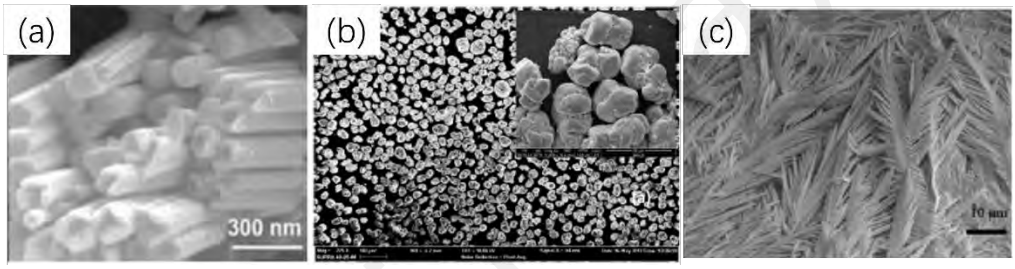

Figure 2.7 (a) High-magnification SEM images of the electrochemically prepared sample (Ref. Li et al., 2012) (b) SEM micrograph of the "as received" tellurium powder (Ref. Coscia et al., 2018) (c) FESEM images of Te films electrodeposited at -0.31V for 300s (Ref. Mu et al., 2018)

For laser modulation applications, Han et al. (2021) showed the passively Q-switched Pr:YLF laser in the orange (605nm), red (639nm), deep red (721nm) spectral ranges with tellurium nanosheets as saturable absorber (SA). They successfully realized the passively Q-switched mode-locked laser at 639nm with the tellurium saturable absorber (SA).

Furthermore, He et al. (2022) reported that tellurium nanowires (Te NWs) synthesized by the hydrothermal method could be used as the tellurium saturable absorber (Te-SA) to realize a femtosecond fiber laser. The saturable intensity and modulation depth were determined to be 8.9MW/cm^2 and 27.0%, respectively.

Furthermore, an Er-doped mode-locked fiber laser with a pulse width of 621fs and an output power of 3.44mW was obtained.

Meanwhile, TeO_2 was prepared on glass and Si substrates through thermal evaporation by Hamdi-Mohammadabad et al. (2022). The TeO_2 coated on glass or Si substrate absorbed in both UV (Ultraviolet) and visible regions. They found that absorption increased as the evaporation temperature increases. The morphology of SEM showed that the number of TeO_2 sheets increases, TeO_2 particles decreases, and the thickness of the film increases with increasing growth temperature.

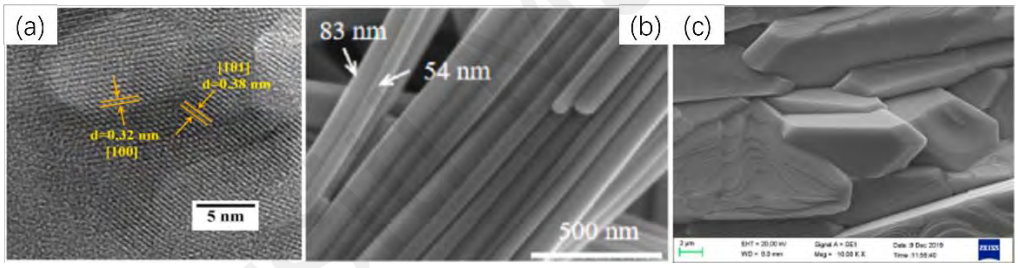

Figure 2.8 (a) TEM images of Te nanosheets synthesized by liquid phase epitaxy and chemical method (Ref. Han et al., 2021) (b) High-magnification SEM images of Te NWs prepared by hydrothermal method (Ref. He et al., 2022) (c) SEM images of TeO_2 thin layers coated on glass substrate at 500℃ by evaporation method (Ref. Mohammadabad et al., 2022)

Furthermore, Liu et al. (2021) explored the thermoelectric performance and feasibility of two-dimensional tellurene, which were used in wearable flexible thermoelectric generators for low-power wearable sensor systems, and power generation clothing. Amazingly, tellurene was found to have a possible ZT_{max}=2.9. Table 2.5 indicates the application of Te materials in photo response, light absorption, and saturable absorber (SA).

Table 2.5 Synthesis of tellurium materials via different routes applied in the field of optic.

Reference	Materials	Methods	Content/Application
Li et al. 2012	Te nanorods	Electrochemical technique	Photoresponse
Coscia et al. 2018	Te/PMMA grains	Dry vibration milling	Optical absorption (310-2200 nm)
Mu et al. 2018	Te films	Electrochemical technique	Strong light absorption in the visible range
Han et al. 2021	Te/PMMA films	Liquid phase epitaxy and chemical	Saturable absorber with optical absorption properties
He et al. 2022	Te nanowires	Hydrothermal	Saturable absorber and ultrafast photonics
Hamdi-Mohammadabad et al. 2022	Te films and nanowires	Evaporation	Optical absorption and microstructural growth

2.3 Summary and research gap

Nowadays, many literatures introduced the enhancement of thermoelectric performance of Te doped with other metal elements or organic additives for modification and even realized TE generator/coolers, sensors, optical absorbers and wearable devices. In these studies, researchers found some factors that affect the thermoelectric properties of Te such as structural defect, carrier concentration, temperature dependence, environmental condition, reaction time. Detailed morphology studies are always neglected; however, actual sample morphology directly affects product performance and application compatibility. Although, sample morphology is dependent on basic parameters, preparation method, doping and additives directly or indirectly. Identical elements exhibit similar properties under similar morphologies regardless of the preparation process of the sample. The electrochemical deposition technique is easier to control its parameters so that we could observe the development of sample morphology in more detail. Therefore, we studied the CV curves of tellurium and morphology of

tellurium films under different conditions via electrodeposition.

CHAPTER 3: METHODOLOGY

3.1 Introduction

In this section, Te films will be synthesized by electrochemical deposition (ECD) technique. Due to most of the p-type materials such as Te has strong anisotropy in the sample growth process and the morphology of the tellurium film usually has branched structures and is relatively sparse. Thick and dense Te films suitable for thermoelectric devices will be studied to find out their relationship with ECD parameters. Although, some anisotropic structures of Te or Te with additives have a huge impact on the sample characteristics and the properties of thermoelectric devices. However, these structures have a good potential to be applied in optical fields or sensors.

Cyclic voltammetry (CV) curves are widely studied in a variety of electrochemical experiments. As one of the unary p-type materials (tellurium) has good advantage whereby the deposition curve can be studied more clearly and carefully in order to optimize the morphology of the film. Additionally, three different additives were identified as polyvinyl alcohol (PVA), tartaric acid (TA) and sodium lignosulfonate (SLS) and will be adopted in this study to manipulate the morphology of as-deposited tellurium films. A rational route to deposit tellurium films with various morphologies will be established.

3.2 Synthesize and characterizations of Te films.

Electrochemical experiments were performed by VersaSTAT3 electrochemical workstation (Princeton Applied Research, USA). Figure 3.1 (a) shows the schematic diagram of the electrochemical cell setup. Tellurium film depositions were performed using a three-electrode system with a platinum (Pt) foil as the counter electrode (CE) and an Ag/AgCl in saturated potassium chloride (KCl) as the reference electrode (RE). The working electrode (WE) consists of a Si substrate covered with a 150 nm thick Si_3N_4 layer and a 100 nm thick gold (Au) conductive layer. During the processing of samples, firstly, the substrates were soaked in a petri dish containing acetone solution for 30 minutes, and then rinsed them with isopropanol (C_3H_8O) or anhydrous ethanol (C_2H_6O) and deionized water (DI) in sequence. Cyclic voltammetry (CV) measurements were performed on the gold (Au) substrate at a scan rate of 0.1V/s.

All tellurium films were synthesized by dissolving 10 mM TeO_2 in an electrolyte consisting of 1 M nitric acid (HNO_3) (6.5 mL) and 0.01 M sodium nitrate ($NaNO_3$) (or additive) and 100mL deionized water (DI) at 60 ℃ for 1.5 hour with centrifugation. In this work, we have separately investigated the effects of three additives (0.01wt% polyvinyl alcohol (PVA), 0.01 M tartaric acid (TA) and 0.2 g/L sodium lignosulfonate (SLS)) on pulse-deposited tellurium. The structural formulas of the additives used are shown in Figure 3.1 (b), (c) and (d). In detail, Table 3.1 shows the Te parameters of electrodeposition, additives dosage and deposition time.

Table 3.1 Te ECD parameters and additives dosage

Bipotential deposition	Te	Te + TA	Te + PVA	Te + SLS
Initial potential	V_{on} = – 0.19V, V_{off} = 0.3V	V_{on} = – 0.225V, V_{off} = 0.3V	V_{on} = – 0.2V, V_{off} = 0.3V	V_{on} = – 0.24V, V_{off} = 0.3V
Optimized potential	V_{on} = 0.05V, V_{off} = 0.3V	V_{on} = 0.07V, V_{off} = 0.3V	V_{on} = – 0.14V, V_{off} = 0.3V	V_{on} = – 0.05V, V_{off} = 0.3V
Deposition time	t_{on} = 10ms, t_{off} = 50ms	t_{on} = 10ms, t_{off} = 50ms	t_{on} = 10ms, t_{off} = 50ms	t_{on} = 10ms, t_{off} = 50ms

When the electrochemical deposition process was completed, the as-grown sample was immediately rinsed with deionized water (DI) to remove the residual electrolyte on the substrate for the subsequent characterization. The different potential samples produced in this study are summarized in Table 3.1. Cyclic voltammetry (CV) for each electrolyte solution (with or without additives) were performed at room temperature in the potential range of – 0.45V to 0.8V. The CV diagram depends strongly on the components of the electrolyte.

The morphology of the electrodeposited tellurium thin films was observed using scanning electron microscopy (SEM) (Hitachi S8100) at a voltage of 10 kV. The crystal orientation of the electrodeposited films was studied using an X-ray diffraction system (XRD) (D2 PHASER). CV curves of tellurium and the fabrication of electrodeposited film were completed using electrochemical workstation (Princeton Applied Research, USA).

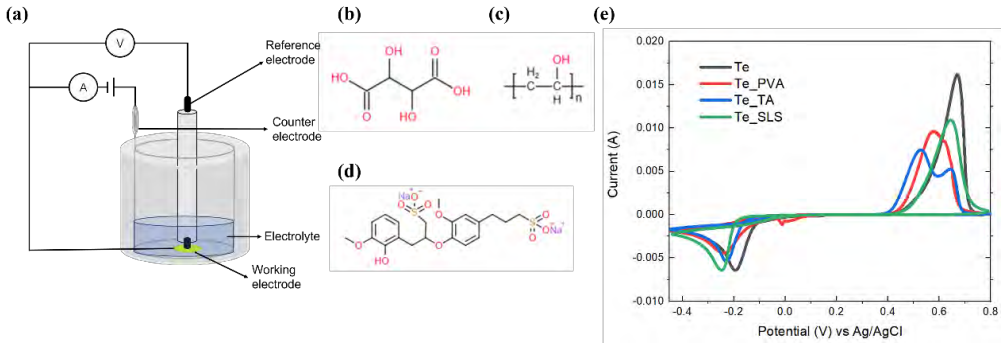

Figure 3.1 Electrochemical deposition of tellurium. (a) Schematic diagram of the three-electrode setup. The structural formula of three additives: (b) tartaric acid (TA). (c) polyvinyl alcohol (PVA). (d) sodium lignosulfonate (SLS). (e) CV curves of tellurium electrolytes with or without additives.

3.3 Chronoamperometry and fast pulse potential method

Chronoamperometry (CA) is to observe current-time dependence with fixed square-wave potential at the working electrode. Chronoamperometry (CA) experiments are commonly used to study electrocatalytic materials, observing the diffusion process occurring at the electrode as a function of analyte concentration. Pulse deposition method has been used to growth of thin films and functional coatings for several years. The method of bipotential fast pulse deposition is used to determine the initial reaction potential V_{on} and the termination reaction potential V_{off}. The corresponding t_{on} and t_{off} are reaction time and resting time. Different from the continuous deposition of chronoamperometry, fast pulse deposition has a period of rest, which has a certain buffering effect on the diffusion process. Compared with the chronoamperometry's fixed potential energy deposition method, the controllable and adjustable bipotential pulse deposition provides a wider and more flexible energy range.

3.4 Preparation of characterization sample

Pretreatment of the deposited tellurium sample before characterization is an essential step. First, a tellurium sample with a smooth surface and metallic luster was selected from a group of samples deposited under the same conditions, as shown in Fig 3.2 (a). Next, as shown in Fig 3.2 (b), the sample was evenly divided into four parts using a silicon scribe, and Figure 3.2 (c) showed the section of sample after being divided. Two pieces of Figure 3.2 (b) were directly used for XRD characterization, and the remaining two pieces were prepared like Figure 3.2 (d) and used for SEM characterization.

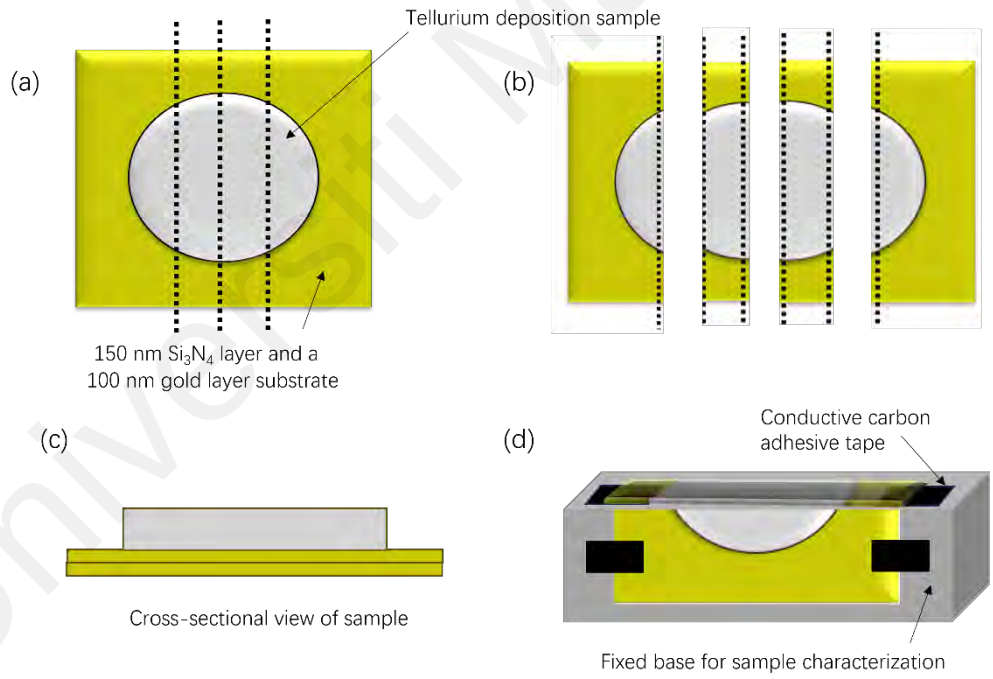

Figure 3.2 Sample preparation and characterization flow chart (a). Overall sample view after electrochemical deposition (b). Split samples using silicone knives (c). Cross-sectional view of sample (d). Characterization sample preparation for SEM

Before SEM characterization, the two pieces of samples divided need to be adhered to both sides of the SEM special base with conductive carbon tape. It is worth mentioning that the sample on the upper side of the SEM special base is used to observe and characterize the surface morphology of the sample. The fixed sample position should be in the center of the SEM special base. The sample pated on the front of the SEM special base is used to observe the cross-sectional morphology of the sample. It should be noted that the divided sample section needs to be consistent with the height of the SEM special base, so that the sample cross-section can be found when the electron microscope is rotated to search. This position does not require excessive adjustment of the electron microscope focus and is conducive to observation. The other two piece of divided samples can be directly used for XRD characterization, we place one of the divided samples into the X-ray cavity. Combing literature and previous experiments, the X-diffractometer was adjusted and determined the glancing angle 2θ=20°-60° with scanning for 10 minutes, and the scanning rate was 4 degrees per minute. Then we use jade software to analyze and determine the consistency of diffraction peaks with sample elements.

CHAPTER 4: RESULTS AND DISCUSSION

4.1 Introduction

The results obtained from all analyses will be shown and discussed in this chapter, including ECD of Te, ECD of Te with additives and the effect of pH. Combined with electrochemical experimental data from Table 3.1, using origin plot to analyze experimental results. SEM was used to observe morphology of the samples and XRD are used to identify the elemental compositions of the samples.

4.2 Electrochemical deposition of tellurium

This part introduces preliminary exploration of ECD of tellurium film, analysis of CV curves for ECD of tellurium, ECD optimization for tellurium film and modification ECD of tellurium film by additives (TA, PVA, SLS)

4.2.1 Preliminary exploration of deposition of tellurium film

In this study, a preliminary investigation on the deposition of tellurium film has been carried out under electrodeposition, chronoamperometry (CA) method and fast pulse potential method. The results are shown and compared in this section.

In the initial stage of the electrodeposition of tellurium, we picked out the deposition potential of – 0.075V and 0.174V. Open circuit voltage (OCV) was around 0.4-0.5V. These parameters are based on the literature. The reduction

reaction deposition time and static time were set as 10ms and 50ms respectively. Tellurium films were deposited at room temperature in acid solution for 10 minutes, 20 minutes and 30 minutes via fast pulse potential method. The surface morphologies of these samples were found to be difference. The thickness of the tellurium film cross-sectional morphology was increased with the extension of deposition time. Many structures of branches are observed in the sectional morphology of tellurium film deposited at 10, 20, 30 minutes as can be seen in Figure 4.1 The surface deposited for 10 minutes is like a flower, the cross-section is only 200-300nm thickness. The growth orientation of crystal grains was anisotropic at 20 minutes. The surface of granular spherulites sample thickness was about 700nm and their average grain diameter is 500 nm. Particles of same sizes can be seen on the surface deposited for 30 minutes; the cross-section branches gradually disappear. The surface of the spherulites and the cross-section of the branched structure are clear under SEM images for 20 minutes.

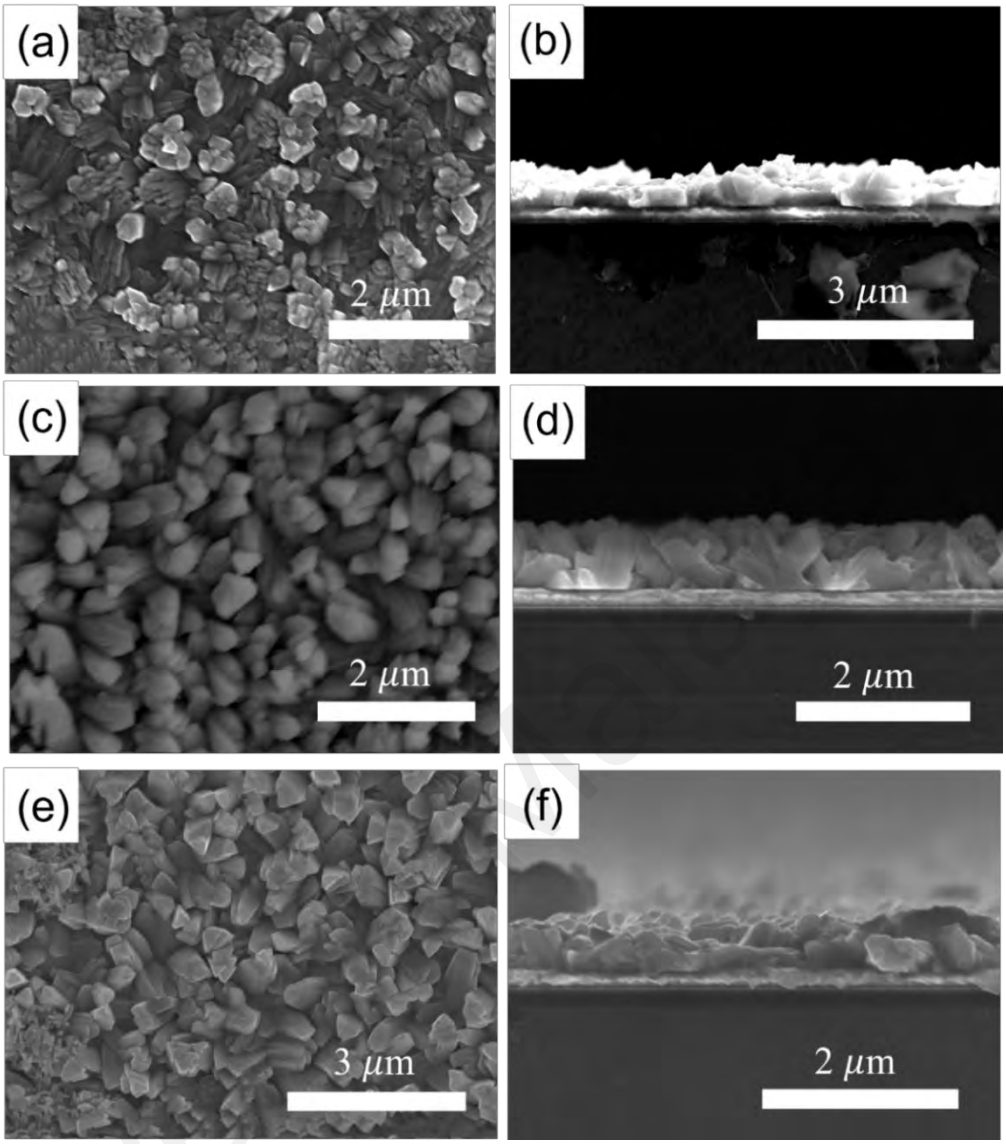

Figure 4.1 Morphology images of electrodeposited tellurium sample at room temperature in 10 mins (a) surface (b) cross-section; 20 mins (c) surface (d) cross-section; 30 mins (e) surface (f) cross-section.

In addition, chronoamperometry method is attempted for deposition of samples, which are grown at a potential of – 0.15V and a reaction time of 10 minutes. The surface morphology is looks like petals of a flower as shown in Figure 4.2. The cross-section of the film is irregular and rough with a thickness of about 200 nm. On top of that, another attempt has been made by using fast potential pulse method at a very small current of 1mA. The pulse time and static time are determined at

10ms and 50ms respectively in all the experiments. Because a pulse time of 10ms with a 1:5 on/off ratio is well-suited for electrodeposited thermoelectric films. (Schumacher et al., 2012) In the electrodeposition process, the cathodic current density is corresponding to the reduction processes of ions during t_{on} and the anodic current density is approximately zero during t_{off}, t_{off} is the rest time for recovering the reactants ions diffusion near the electrode surface, reducing the concentration polarization near the cathode. (Esmailzadeh et al., 2021)

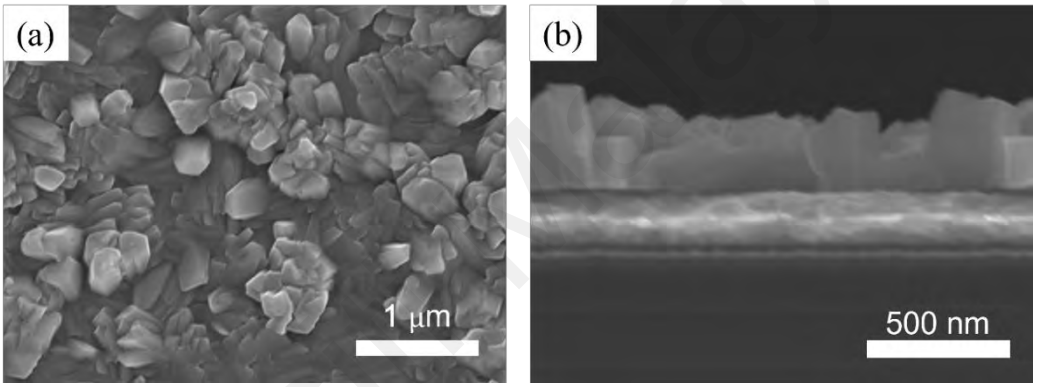

Figure 4.2 Morphology images of chronoamperometry tellurium sample at room temperature in 10 mins (a) surface (b) cross-section

Compared with the chronoamperometry and fast pulse potential method, thickness of sample cross-sections varies significantly. The cross-section of the sample has a thickness of 2-3μm by fast pulse potential in Figure 4.1 and the cross-section of the sample has a thickness of 500nm by chronoamperometry. Here is an analysis of why there is such a big difference, the concentration of solution ions in the electrolyte decreases with the deposition time increases. It would require more energy for the current to carry the same amount of electrolyte as during the initial deposition. However, the potential (energy) is constant (chronoamperometry), on the one hand, the amount of electrolyte carried by the current will decreases due

to insufficient energy. On the other hand, with the reduction of metal ions, the conductivity of solution becomes worse and the current naturally decreases. Perhaps, the combination of these two aspects makes electrochemical deposition more difficult to occur. From the pulse deposition method, it can be concluded that the current gradually becomes smaller and basically reaches a stable state after 30 minutes of deposition. Fast pulse potential can provide energy more flexibly according to changes in current during the process. We can obtain the current changes during actual deposition under fast pulse potential. This may be one of the reasons why the film thickness is thicker compared with the chronoamperometry method at the same time (10 minutes). In terms of surface morphology, spherulites appear more frequently under fast pulse potential in Figure 4.1 (a), and petal-shaped ones appear more frequently under the chronoamperometry in Figure 4.2 (a). The thickness of deposited films by the different methods are different, as shown in Figure 4.1 (b) and Figure 4.2 (b).

4.2.2 Analysis of CV curves for ECD of tellurium

In general, CV curves are important research tools for observing and studying electrochemical deposition. In previous studies, researchers typically used the first three CV cycles to determine an appropriate deposition potential. (Schumacher, 2012; & Schumacher, 2013) However, the deposition potential from the literature cannot achieve the ideal deposition morphology very well. We redesigned the experiment to observe the change of the tellurium CV curve with and without

additives via the fast pulse potential method. Figure 3.1 (e) shows the CV curves of tellurium with and without additives. As shown in Figure 3.1 (e), different additives produce different peak potentials and current densities. The peak potential of tellurium, tellurium with TA, tellurium with PVA and tellurium with SLS are – 0.19V, – 0.225V, – 0.2V and – 0.24V respectively. When the surfactants are added to the electrolyte, the current density decreases. This can be explained by the absorption of the surfactant molecules on the surface of the electrode, which decreases the current density. The part of organic molecules is adsorbed on the the metal electrode surface through spontaneous organization into monolayers (Aranzales et al., 2021), resulting in weaker ion migration, weaker current and more negative deposition potential.

In order to investigate the evolving process of CV curves as functions of the deposition time, a reference experiment was designed and successfully completed to monitor the CV characteristics intermittently during the deposition process. For instance, for the tellurium electrolyte, we applied pulsed deposition parameters at V_{on} = – 0.19V, t_{on} = 10ms, V_{off} = 0.3V, t_{off} = 50ms. In order to avoid the unnecessary dissolution of the deposited material, V_{on} and V_{off} represent the reaction initiation and termination potentials, respectively. The CV curves of intermetallic compounds recorded in the negative potential direction from – 0.45V to 0.3V. As shown in Figure 4.3 (a), both the peak deposition potential and current decreases with the increase of deposition pulses. Figure 4.3 (b) shows the peak deposition potential as a function of pulse number. At the first 10000 pulses (10 minutes), the peak deposition potential dropped rapidly. However, it was observed

that the number of pulses gradually saturated from 20000 to 60000 (20-60 minutes). A series of experiments were performed on tellurium electrolytes with different additives, namely TA, PVA and SLS. As shown in Figure 4.3 (b), all three tellurium electrolytes exhibit similar phenomenon with the CV curves generally becoming stable after 10000 cycles. Herein, we define the peak potential obtained by the first three CV cycles as the "initial potential" and defined the saturated peak potential after a certain period of deposition as the "stabilized potential".

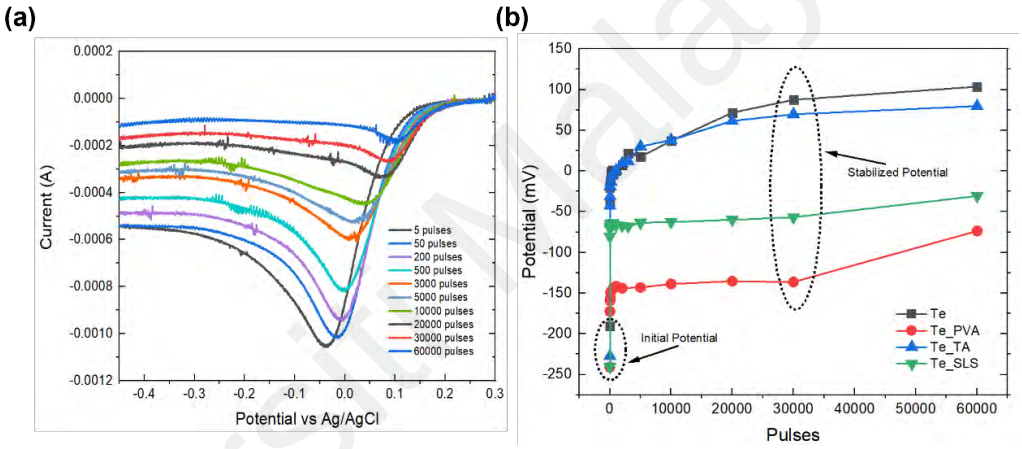

Figure 4.3 CV curves of tellurium with and without additives. (a) CV curves of tellurium without additives for different deposition pulse numbers; (b) Plot of peak deposition potential as functions of pulse numbers for tellurium with and without additives.

This is an important finding because previously researchers only selected their deposition potentials based on the first three CV cycles. As shown in Figure 4.3, the deposition curve changes drastically with the increasing electrochemical deposition time in the tellurium system. Therefore, dynamical control of the deposition potential should be applied in the real electrochemical deposition process. A possible explanation for the different deposition potentials and currents are proposed as follows:

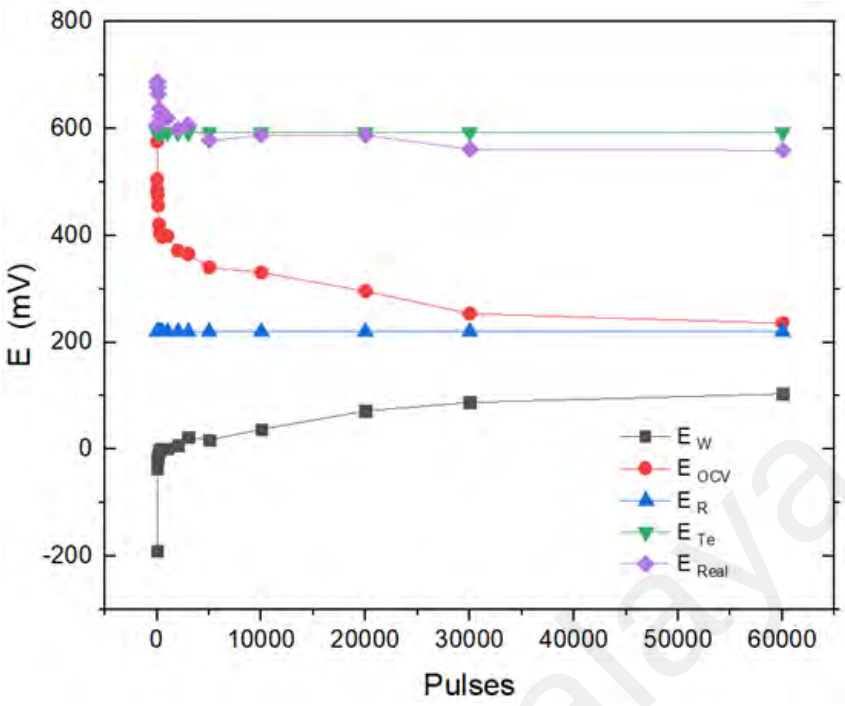

Figure 4.4 The relationship between deposition pulses and various potentials

The conversion of energy throughout the system can be shown in Figure 4.4. The relationship between the multiple energy sources in the whole system is shown in the formula: $E_{OCV} + E_R + E_W = E_{Real}$, where E_{Real} is the total amount of actual energy in the system, E_{OCV} is the open circuit voltage (OCV) of Au surface, E_R is the potential of the reference electrode (RE), E_W is the applied potential of the working electrode (WE), and E_{Te} is the electrochemical-reduction potential required for the tellurium reaction, which is typically in the range of 0.55V to 0.6V depending on the reference electrode (RE) (Abad et al., 2015).When the energy values of E_{Real} and E_{Te} coincide with or are close to each other, the electrochemical deposition of tellurium is more likely to be fully deposited. For tellurium electrolyte without additives, the E_{OCV} is between 0.4V and 0.5V resulting from the difference between the ionic potential of the electrolyte solution and the work

function of gold relative to the Ag/AgCl reference electrode (RE). The Ag/AgCl electrode is 0.22V relative to the standard electrode. Therefore, the initial E_W needs to be traced back to negative range potentials to achieve the tellurium deposition. After a period of deposition, on the one hand, the current transport through the substrate become weaker because the gold substrate is covered with a tellurium layer. On the other hand, the decrease in the concentration of the electrolyte solution and the decrease in ion concentration affect the conductivity of the solution, the conductivity becomes weaker and the current decreases. There is a high probability that they joint caused the decline of E_{OCV}, but E_{Te} required electrochemical-reduction potential of tellurium remains unchanged. Thus, E_W requires more energy to satisfy the reduction potential of tellurium deposition, which is why it moves in the positive direction (E_W). Finally, the energy required for the reaction tends to be stable when the tellurium completely covers the gold (Au) surface, and the applied potential (E_W) remains basically unchanged after a period of deposition.

4.2.3 Optimization ECD of tellurium film

Since the deposition curves move to the positive direction during the long-term electrochemical reaction (Figure 4.3 (a)), the shift of the peak potential will affect the sample deposition process as the deposition time increases. As shown in Figure 4.3 (b), after a certain reaction time, the peak potential of the sediment stabilized, indicating that the electrochemical reaction is uniform and stable at this

potential. Therefore, it is hypothesized that tellurium film growth at this stable deposition potential should have thick and homogeneous morphology.

In these experiments, we designed and applied a pulsed deposition protocol. During the preparation of thin films by galvanostatic and potentiostatic methods, the reducible species near the working electrode will be rapidly consumed. If the remaining reducible ions in the electrolyte cannot diffuse to the vicinity of the working electrode (WE) in time, this may lead to a porous and loose structure. In contrast, pulsed deposition can take advantage of the "off" time, during the closure period, target ions of interest diffuse to the working electrode (WE), thereby restoring the concentration of these ions. In the experiments, V_{on} and V_{off} represent the reaction initiation and termination potentials, respectively, and t_{on} and t_{off} represent the duration. V_{on} represents the deposition potential, and V_{off} is the static potential at which the current is approximately zero. t_{on} and t_{off} indicate the turn-on and turn-off time of pulse deposition, they correspond to 10ms and 50ms, respectively. From the previous experiments, a pulse time of 10ms and an on/off ratio of 1:5 is well suited for electrodeposition of thermoelectric thin films. (Schumacher et al., 2012)

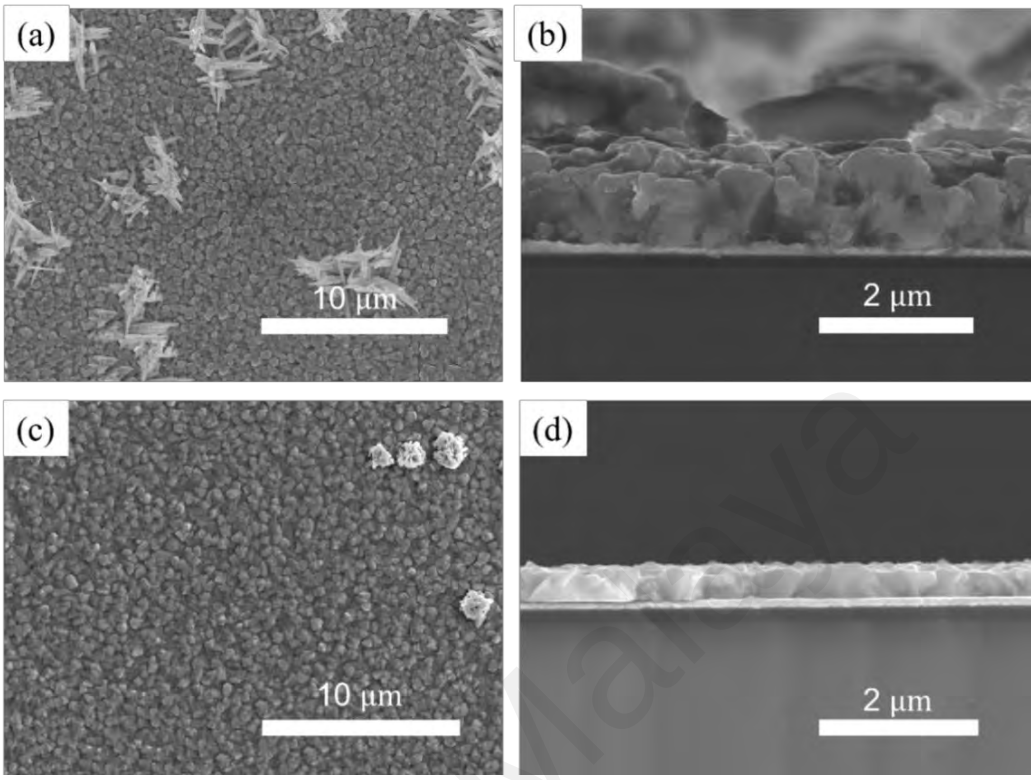

Figure 4.5 Morphology of tellurium deposited at the initial potential of -0.19V (a) surface (b) cross-section; at the stabilized potential of 0.05V (c) surface (d) cross-section.

In order to observe the effect of different deposition potentials on the morphology of tellurium thin films, we compared the morphology of tellurium thin films (V_{on}) fixed at the initial or stabilized potential. The comparison of the surface and cross-sectional morphology of tellurium films prepared at initial potential (– 0.19V) and stable potential (0.05V) is shown in Figure 4.5. As shown in Figure 4.5, the surface of the tellurium samples has a metallic luster prepared by a stable potential. Combining Figure 4 (a) and (b), the morphology of tellurium films prepared at stable potential of 0.05V is denser than that deposited at an initial potential of – 0.19V, as shown in Figure 4.5 (c) to (d).

The crystal nucleus grows rapidly due to sufficient energy, resulting in some 1-4μm large and branched crystal structures at the initial potential. The crystal nucleus grows strongly in all directions under the stimulation of energy, resulting in a sparse underlying film. Due to the influence of coarse crystals, the cross-section shown in Figure 4.5 (b) is rough and wavy. However, relatively slow nucleation growth was observed for samples grown at a stable potential. This results in a flatter plane of smaller grain and a denser cross-sectional morphology. Figure 4.5 (c) shows only a few allotropic spherulites with a diameter of 2μm. During deposition, most spherulites have a diameter of 300-500nm at a steady potential. Depending on the sample morphology, it can be demonstrated that when using a selected stable potential, the deposited tellurium film can be thicker and more homogeneous than the initial potential. Therefore, based on the phenomenon that the CV curves shifts to right, this approach could help us obtain better sample morphology than the general way.

4.2.4 Modification ECD of tellurium film by additives

Although dense and compact tellurium films are a prerequisite for building up on-chip integrated micro thermoelectric devices (Li et al., 2018), tellurium films with dendritic morphology might be very attractive in applications of piezo electronics (Apte et al., 2021), gas sensors (Yuan et al., 2022) or photodetectors (Khosravi-Nejad et al., 2019). One of the strategies is that improving the morphology of tellurium films with the different additives during electrodeposition. Additives can

effectively control and increase the surface energy of specific crystal structures (Kondalkar, et al., 2014). In this work, we investigated the effect of three different additives, tartaric acid (TA), polyvinyl alcohol (PVA), and sodium lignosulfonate (SLS). In the previous studies done by other researchers, high concentrations of additives can easily change the CV curve of tellurium, so it is difficult to study the real effect of additives when the deposition potential is changed (Abad, 2015; Schoenleber, 2014; Sabran, 2019). To minimize the effect of this condition, a series of concentration screening experiments were performed. In the end, it was found that 0.01M tartaric acid (TA), 0.01wt% polyvinyl alcohol (PVA) and 0.2g/L sodium lignosulfonate (SLS) were the optimal additive concentrations for the deposition of tellurium system at room temperature.

As shown in Figure 3.1 (b), the molecular structure of tartaric acid (TA) consists of hydroxyl groups. In this experiment, 0.01M tartaric acid (TA) was added to the tellurium electrolyte and the results were shown in Figure 4.6. Similar for the tellurium deposition, the sample with TA were electrodeposited at initial and stable potentials. Figure 4.6 (a) and (b) show the SEM images of the as-deposited tellurium films under the initial potential of – 0.225V, while Figure 4.6 (c) and (d) show the SEM images of the tellurium film at the steady potential of 0.07V. Compared with the morphology of initial potential (– 0.225V) in Figure 4.6 (a) and (b), the morphology of tellurium film with TA shown in Figure 4.6 (c) and (d) at a stable potential of 0.07V resulted in smaller crystal grains and a denser film. In Figure 4.6 (a), many anisotropic branched structures can be seen on the surface of the film, while in Figure 4.6 (c), cubic crystals and spherulites of 500-700nm

are the main structures. It can be seen from the cross-section that one or more layers of film are spread unevenly on the gold surface. The cubic crystals and spherulites produced by the stable potential are denser in cross-section than the grass-like structure of the initial potential from. Although, the grass-like structure in Figure 4.6 (b) has a negative impact on the thermoelectric performance. However, this grass-like morphology can be an effective structure for photodetectors (Khosravi-Nejad et al., 2019).

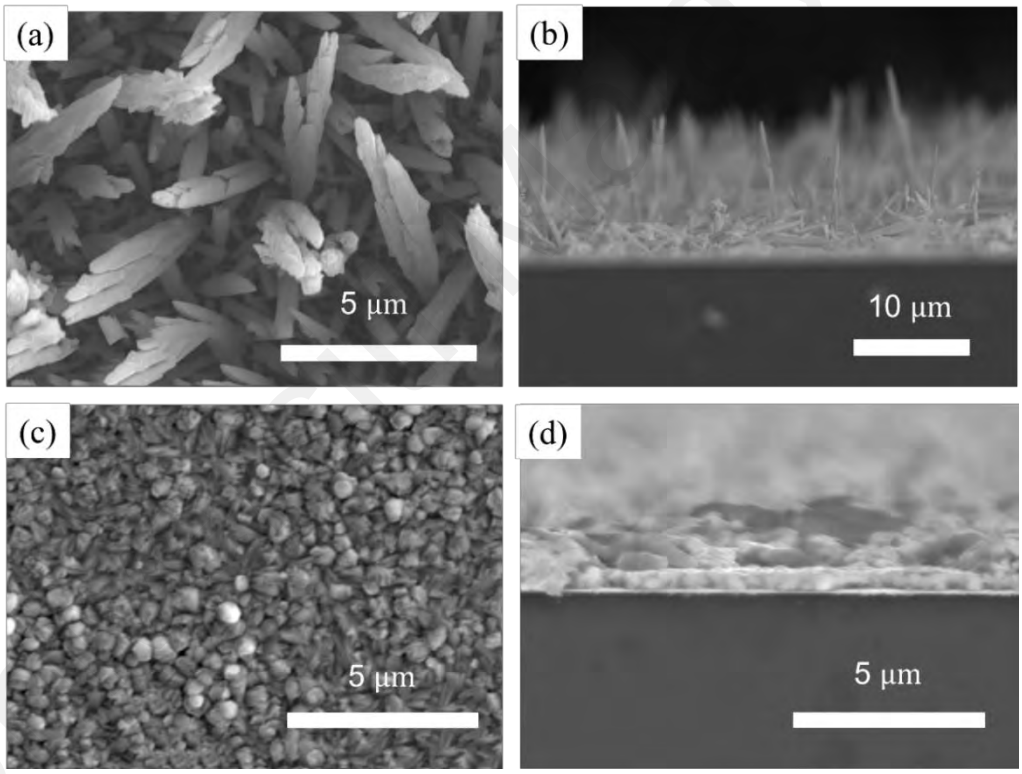

Figure 4.6 Morphology of tellurium with TA deposited at the initial potential of – 0.225V (a) surface (b) cross-section; at the stabilized potential of 0.07V (c) surface (d) cross-section.

Meanwhile, PVA is an organic additive due to the hydroxyl group in its chemical structure as shown in Figure 3.1 (c). The compound in the electrolyte dissociates stably and release metal cations at chemical equilibrium potential. The polar hydroxyl groups of the polymer chain form intermolecular and intramolecular

hydrogen bonds with transition metal ions. Therefore, the addition of PVA to tellurium electrolytes might result in microstructures with uniform grains (Tishkevich et al., 2018). The morphology results of tellurium films with PVA additives are shown in Figure 4.7. Figure 4.7 (a) and (b) show the results of tellurium film at the initial potential of – 0.2V, the cross section become thicker but not quite flat. Figure 4.7 (c) and (d) show the morphology under stabilized potential of – 0.14V, the film becomes thicker and uniform in the cross-section. As seen in Figure 4.7, the deposited tellurium films with PVA additives are more like mattress structures. Electrodeposition with PVA additives show smaller grains compared to the results with TA as the additives, and the cross-section view of the tellurium films shows colloidal structures. The colloidal structure might make up for the holes in the film to a certain extent, which is more conducive to making the film denser. The reason the film becomes thicker and denser is because the repeating structural units of the polar polymer form a regular structure, allowing the anions to be evenly distributed throughout the substrate.

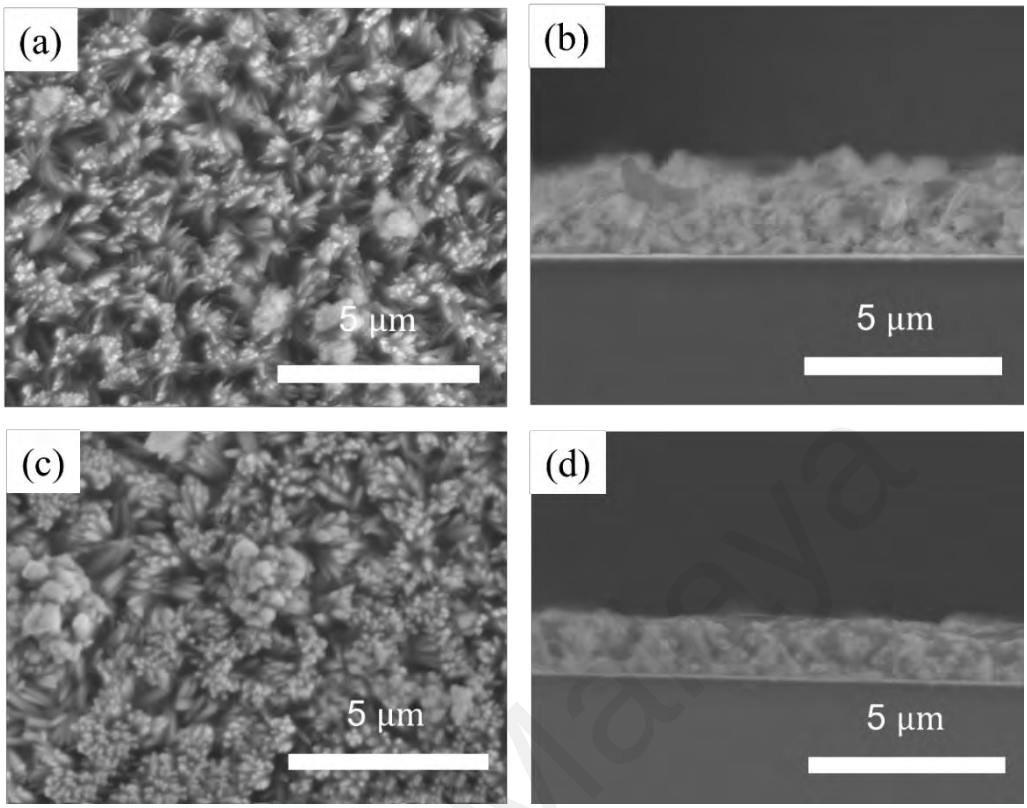

Figure 4.7 Morphology of tellurium with PVA deposited at the initial potential of – 0.2V (a) surface (b) cross-section; at the stabilized potential of – 0.14V (c) surface (d) cross-section.

Lastly, Sodium lignosulfonate (SLS) a natural polymer, is one of the anionic surfactants (Caballero-Calero et al., 2014), and its structure is shown in Figure 3.1 (d). Published reports of successful use of SLS as additive enhance film properties (Abad et al., 2015), improve morphology (Caballero-Calero et al., 2015) and optimize bath (Caballero-Calero et al., 2018) of the film. Hence, the idea arose to study the effect of SLS on the morphology of single electrodeposited tellurium films. It has strong dispersive adhesion and can adsorb solids on the surface. The metal tellurium ions in the compound can be exchanged with the hydrophilic group of sodium lignosulfonate (SLS). There are active groups (such as hydroxyl) inside its structures, which can form condensation or hydrogen bonds with other

compounds. As shown in Figure 4.8 (c) and (d), tellurium added with sodium lignosulfonate (SLS) at a stabilized potential (– 0.05V), a denser film with homogeneous surface was prepared compared to the film obtained with the initial potential (– 0.24V) as in Figure 4.8 (a) and (b). The morphology of the tellurium with SLS film produced at the initial potential is more like needle-like grass. Compared with the tellurium film without additives, the tellurium with SLS film at the stabilized potential will be thicker in cross-section.

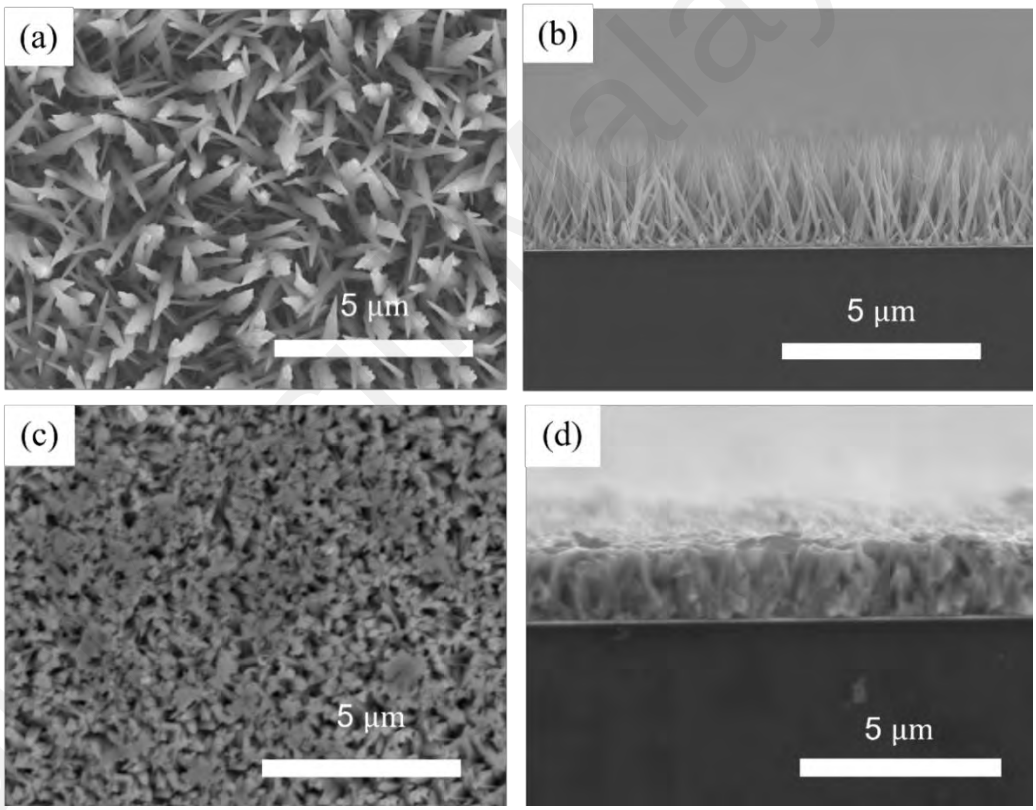

Figure 4.8 Morphology of tellurium with SLS deposited at the initial potential of – 0.24V (a) surface (b) cross-section; at the stabilized potential of – 0.05V (c) surface (d) cross-section.

The possible mechanism of the influence of three additives on the film morphology can be summarized. In general, the additives in the electrolyte have certain influence on ion diffusion, which also explains the relatively higher reduction potentials of the CV curves of the tellurium electrolytes with additives, as shown in Figure 3.1 (e) (Schoenleber et al., 2014). Therefore, tellurium thin films with additives are likely to grow in dendritic manners. In addition, the molecule structure of additives can also affect the film morphology, which will be further investigated in our future research.

4.3 Effect of pH

The electrolyte pH adjustment has been considered to improve the morphology of tellurium. Using ammonia-water ($NH_3 \cdot H_2O$) to adjust the pH value in the electrodeposition experiments. Peak deposition potential shift occurred when pH was adjusted, the current density drops, and pH value rises in Figure 4.9 (a) and (b). Poor deposition effect was obtained by changing pH value at the same deposition time with or without additive. When the pH value is adjusted to 1-2, the adhesiveness of the tellurium with PVA film get worse. The film is more likely to fall off and only the substrate is left, when the sample is taken out and rinsed by deionized water. The pH-adjusted tellurium films deposited with or without additives are very thin and poorly absorbent. The film surface no longer has a bright metallic luster and turns dark. Additionally, it is easy to observe under the same magnification in the SEM image of Te-PVA that the unadjusted pH sample has fewer and concentrated crystal bundles in Figure 4.9 (c), while the pH adjusted

sample has more surface crystal bundles in Figure 4.9 (d). Overall, changing the pH of electrolyte is not a good choice to optimize the film morphology of tellurium and tellurium with additives.

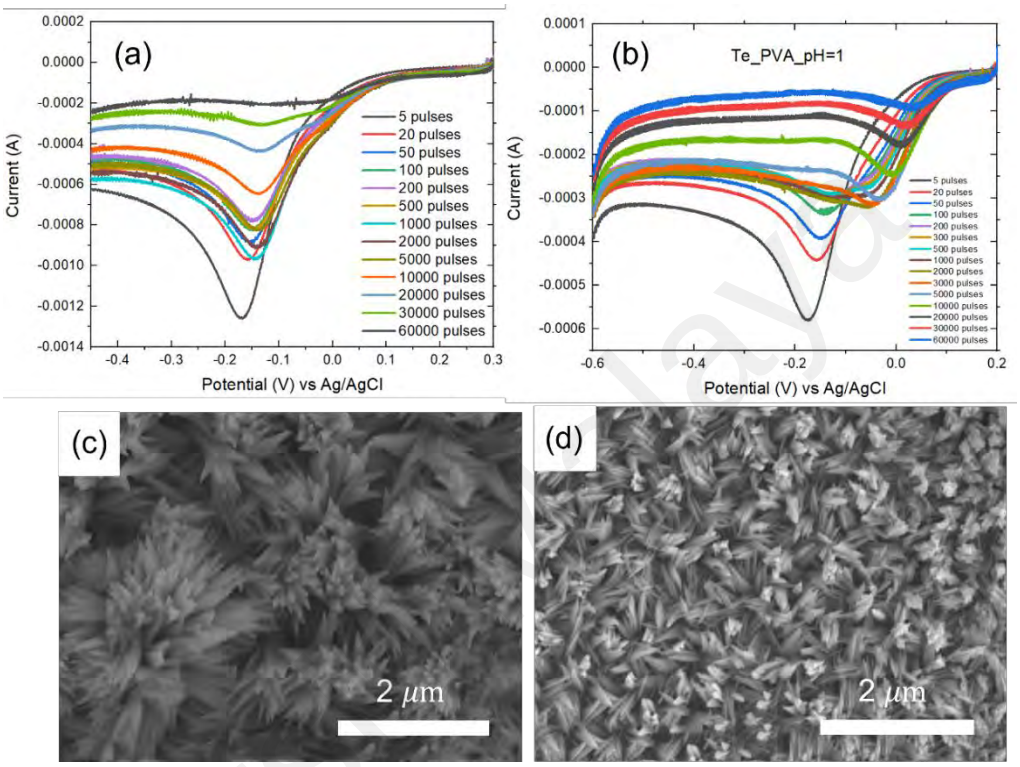

Figure 4.9 CV and SEM images of pH-adjusted tellurium-added PVA (a). CV with unadjusted pH (b) CV with a pH adjustment of 1 (c). SEM image of unadjusted pH (d). SEM image of pH value adjusted to 1.

4.4 XRD analysis

Structural analysis of tellurium films was characterized by X-ray diffractometer (XRD), scanning at glancing angle of 2θ=20°– 60° for 10 minutes. Figure 4.10 shows the X-ray diffraction (XRD) patterns of tellurium thin films with and without various additives at different potentials. Different diffraction peaks are observed, which were assigned as a reference (JCPDS 78-2312) for tellurium. The diffraction peak at 2θ=27.551° is due to the (101) tellurium crystal place. The second order diffraction peak at 2θ=45.878° and the (003) place also can be seen

in the diffraction pattern. Meanwhile, the diffraction peak observed for gold at (111) matches that of the reference (JCPDS 04-0784), due to the gold (Au) substrate are used in the electrodeposition. The diffraction peaks at (101) of the samples with additives at the stabilized potential are sharper than that at the initial potential from Figure 4.10 (a) and (b). Moreover, the addition of additives at the stabilized potential reduces the intensity of the diffraction peak at (003). This indicates that most grains grow along the (101) direction, especially at stable potential. The initial potentials are usually more negative than the stabilized potentials for both with and without additives, which might lead to anisotropic growth of tellurium films. In addition, the additives in the electrolytes could also be adsorbed on the surface of the tellurium layer, affecting the deposition current and potential, and eventually modifying morphology of the film. The stable deposition peak potentials are chosen when the reaction process tends to stabilize. Since the reactions are uniform and smooth at the stabilized potential, the grains tend to grow uniformly, and the films become denser as a result.

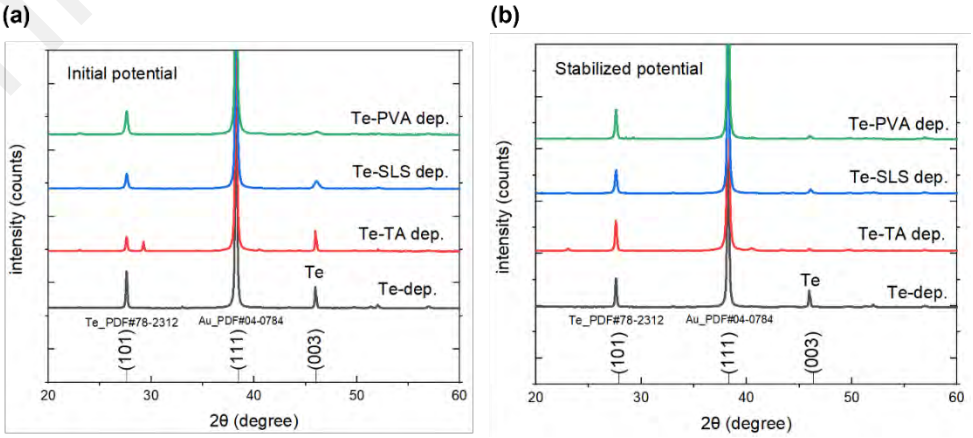

Figure 4.10 XRD patterns of tellurium film produced with and without additives: (a) at initial potential, (b) at stabilized potential.

CHAPTER 5: CONCLUSION

In this work, a study on the cyclic voltammetry (CV) of tellurium by electrochemical deposition (ECD) experiments was carried out to improve its film morphology. It was found that the CV curve shifted in the positive direction as the duration of tellurium electrodeposition increase. Based on this situation, the effects on the tellurium film morphology were investigated at the initial and stabilized deposition potential with or without the additives. According to the results obtained, the conclusions are described.

Based on the CV curve, stabilized potential was used to deposit the sample, it was found by SEM that the sample morphology was improved compared to the initial potential. CV can record the deposition process very well. The initial potential is directly getting the initial grains deposited on the gold substrate, but as the grains are deposited layer by layer and deposition time increase, the change of deposition potential is visually seen on the CV curve. This is due to the reason why the particles are not directly deposited on the substrate but gradually deposited on the deposition layer. Finally, the potential is basically constant, and this potential is called a stable potential, which is the reason why it is more suitable for optimizing the morphology of long-term deposition sample.

Different additives could produce different sample morphology. Some additives adsorbed on the electrode surface affect the sample morphology by affecting the deposition potential. In addition, additives also may directly replace or combine with the functional groups of the electrolyte, which will affect the sample

morphology. As far as the morphology is concerned, PVA additives have more advantages in sample morphology optimization, which are more uniform, homogeneous, and repeatable.

REFERENCES

Abad, B.; Rull-Bravo, M.; Hodson, S. L.; Xu, X.; Martin-Gonzalez, M., Thermoelectric properties of electrodeposited tellurium films and the sodium lignosulfonate effect. *Electrochimica Acta* (2015), *169*, 37-45./10.1016/j.electacta.2015.04.063

Apte, A.; Kouser, S.; Safi Samghabadi, F.; Chang, L.; Sassi, L. M.; Litvinov, D.; Yakobson, B. I.; Puthirath, A. B.; Ajayan, P. M., Piezo-response in two-dimensional α-Tellurene films. *Materials Today* (2021), *44*, 40-47./https://doi.org/10.1016/j.mattod.2020.10.030

Aranzales, D.; Briliani, I.; McCrum, I. T.; Wijenberg, J. H. O. J.; de Vooys, A. C. A.; Koper, M. T. M., The effect of naphthalene-based additives on tin electrodeposition on a gold electrode. *Electrochimica Acta* (2021), *368*, 137606./https://doi.org/10.1016/j.electacta.2020.137606

Bakthavatchalam, B.; Habib, K.; Saidur, R.; Saha, B. B., Cooling performance analysis of nanofluid assisted novel photovoltaic thermoelectric air conditioner for energy efficient buildings. *Applied Thermal Engineering* (2022), *213*, 118691./https://doi.org/10.1016/j.applthermaleng.2022.118691

Bo, X.; Tang, A.; Dou, M.; Li, Z.; Wang, F., Controllable electrodeposition and mechanism research of nanostructured Bi2Te3 thin films with high thermoelectric properties. *Applied Surface Science* (2019), *486*, 65-71./10.1016/j.apsusc.2019.04.194

Caballero-Calero, O.; Borca-Tasciuc, D.-A.; Martínez-Moro, R.; Gorog, A.; Mohner, M.; Borca-Tasciuc, T.; Martín-González, M., Improvement of Seebeck coefficient in as-grown Bi2Te3-ySey electrodeposited films by the addition of additives and bath optimization. *Electrochimica Acta* (2018), *269*, 490-498./https://doi.org/10.1016/j.electacta.2018.03.025

Caballero-Calero, O.; Díaz-Chao, P.; Abad, B.; Manzano, C. V.; Ynsa, M. D.; Romero, J. J.; Rojo, M. M.; Martín-González, M. S., Improvement of Bismuth Telluride electrodeposited films by the addition of Sodium Lignosulfonate. *Electrochimica Acta* (2014), *123*, 117-126./https://doi.org/10.1016/j.electacta.2013.12.185

Caballero-Calero, O.; Mohner, M.; Casas, M.; Abad, B.; Rull, M.; Borca-Tasciuc, D. A.; Martín-González, M., Improvements on Electrodeposited Bi2Te3-ySey Films by Different Additives. *Materials Today: Proceedings* (2015), *2* (2), 620-

628./https://doi.org/10.1016/j.matpr.2015.05.087

Cabrera, R. Q.; Latimer, E. R.; Kafizas, A.; Blackman, C. S.; Carmalt, C. J.; Parkin, I. P., Photocatalytic activity of needle-like TiO2/WO3−x thin films prepared by chemical vapour deposition. *Journal of Photochemistry and Photobiology A: Chemistry* (2012), *239*, 60-64./https://doi.org/10.1016/j.jphotochem.2012.05.002

Chen, L.; Lorenzini, G., Comparative performance for thermoelectric refrigerators with radiative and Newtonian heat transfer laws. *Case Studies in Thermal Engineering* (2022), *34*, 102069./https://doi.org/10.1016/j.csite.2022.102069

Choi, J.; Lee, J. Y.; Lee, H.; Park, C. R.; Kim, H., Enhanced thermoelectric properties of the flexible tellurium nanowire film hybridized with single-walled carbon nanotube. *Synthetic Metals* (2014), *198*, 340-344./https://doi.org/10.1016/j.synthmet.2014.10.037

Chuai, R.; Zhang, B.; Yang, Y.; Jiang, G.; Zhang, H.; Li, X., A capacitive pressure-sensitive chip with linkage film. *Microelectronics Journal* (2021), *118*, 105313./https://doi.org/10.1016/j.mejo.2021.105313

Coscia, U.; Ambrosone, G.; Palomba, M.; Binetti, S.; Le Donne, A.; Siliqi, D.; Carotenuto, G., Photoconductivity of tellurium-poly(methyl methacrylate) in the ultraviolet–visible-near infrared range. *Applied Surface Science* (2018), *457*, 229-234./https://doi.org/10.1016/j.apsusc.2018.06.221

Du, Y.; Qiu, G.; Wang, Y.; Si, M.; Xu, X.; Wu, W.; Ye, P. D., One-Dimensional van der Waals Material Tellurium: Raman Spectroscopy under Strain and Magneto-Transport. *Nano Letters* (2017), *17* (6), 3965-3973./10.1021/acs.nanolett.7b01717

El-Makaty, F. M.; Ahmed, H. K.; Youssef, K. M., Review: The effect of different nanofiller materials on the thermoelectric behavior of bismuth telluride. *Materials & Design* (2021), *209*, 109974./https://doi.org/10.1016/j.matdes.2021.109974

Esmailzadeh, S.; Shahrabi, T.; Yaghoubinezhad, Y.; Darband, G. B., An analytical study on nucleation and growth mechanism of nanostructured Ni-Se coating by the chronoamperometry and pulse potential techniques. *Journal of Electroanalytical Chemistry* (2021), *881*, 114949./https://doi.org/10.1016/j.jelechem.2020.114949

Gan, Y. X.; Sweetman, J.; Lawrence, J. G., Electrodeposition and morphology analysis of Bi–Te thermoelectric alloy nanoparticles on copper substrate. *Materials Letters* (2010), *64* (3), 449-452./10.1016/j.matlet.2009.11.045

Gao, J.; Liu, C.; Miao, L.; Wang, X.; Li, C.; Huang, R.; Chen, Y.; Tanemura, S., Power factor enhancement via simultaneous improvement of electrical conductivity and Seebeck coefficient in tellurium nanowires/reduced graphene oxide flexible thermoelectric films. *Synthetic Metals* (2015), *210*, 342-351./https://doi.org/10.1016/j.synthmet.2015.10.018

Ge, Z.-H.; Nolas, G. S., Purification and crystal growth of single-crystalline tellurium tubes and rods. *Materials Letters* (2017), *194*, 20-22./https://doi.org/10.1016/j.matlet.2017.01.137

Glatz, W.; Durrer, L.; Schwyter, E.; Hierold, C., Novel mixed method for the electrochemical deposition of thick layers of Bi2+xTe3−x with controlled stoichiometry. *Electrochimica Acta* (2008), *54* (2), 755-762./10.1016/j.electacta.2008.06.065

Hamdi-Mohammadabad, P.; Tohidi, T.; Talebzadeh, R.; Mohammad-Rezaei, R.; Rahmatallahpur, S., Evaluation of structural and optical properties of TeO2 nano and micro structures grown on glass and silicon substrates using thermal evaporation method. *Materials Science in Semiconductor Processing* (2022), *139*, 106363./https://doi.org/10.1016/j.mssp.2021.106363

Han, L.; Yang, Z.; Yang, Q.; Ren, X.; Zhang, X.; Zhang, B.; Yang, K.; He, J.; Li, C.; Wang, J., Visible nonlinear optical properties of tellurium and application as saturable absorber. *Optics & Laser Technology* (2021), *137*, 106817./https://doi.org/10.1016/j.optlastec.2020.106817

He, P.; Hu, X.; Hu, Z.; Chen, J.; Xie, Z.; Huang, J.; Tao, L.; Lu, H.; Hao, M., Preparation of tellurium nanowires and its application in ultrafast photonics. *Journal of Luminescence* (2022), *252*, 119335./https://doi.org/10.1016/j.jlumin.2022.119335

Hegde, G. S.; Prabhu, A. N.; Gao, Y. H.; Kuo, Y. K.; Reddy, V. R., Potential thermoelectric materials of indium and tellurium co-doped bismuth selenide single crystals grown by melt growth technique. *Journal of Alloys and Compounds* (2021), *866*, 158814./https://doi.org/10.1016/j.jallcom.2021.158814

Hwang, T.-Y.; Song, Y.; Kim, S.; Lee, J.; Eom, N. S. A.; Kwon, Y.-T.; Ryu, S. H.; Park, Y.-K.; Cho, H.-B.; Choa, Y.-H., Rice-like tellurium thin films deposited by a galvanic displacement reaction

and ultra-high sensing response to hydrogen sulfide (H2S) gas at room temperature. *Sensors and Actuators B: Chemical* (2019), *282*, 756-764./https://doi.org/10.1016/j.snb.2018.11.075

Janak, L.; Ancik, Z.; Vetiska, J.; Hadas, Z., Thermoelectric Generator Based on MEMS Module as an Electric Power Backup in Aerospace Applications. *Materials Today: Proceedings* (2015), *2* (2), 865-870./https://doi.org/10.1016/j.matpr.2015.05.112

Kang, S.; Dai, T.; Dang, S.; Ma, X.; Wang, G.; Li, H.; Hu, P.; Yu, F.; Zhou, X.; Wu, S.; Li, S., Broadband photoresponse of tellurium nanorods grown by molecular beam epitaxy. *Chemical Physics Letters* (2019), *729*, 49-53./https://doi.org/10.1016/j.cplett.2019.05.026

Karalis, G.; Tzounis, L.; Mytafides, C. K.; Tsirka, K.; Formanek, P.; Stylianakis, M.; Kymakis, E.; Paipetis, A. S., A high performance flexible and robust printed thermoelectric generator based on hybridized Te nanowires with PEDOT:PSS. *Applied Energy* (2021), *294*, 117004./https://doi.org/10.1016/j.apenergy.2021.117004

Khosravi-Nejad, F.; Teimouri, M.; Jafari Marandi, S.; Shariati, M., The highly crystalline tellurium doped ZnO nanowires photodetector. *Journal of Crystal Growth* (2019), *522*, 214-220./https://doi.org/10.1016/j.jcrysgro.2019.06.020

Kondalkar, V. V.; Mali, S. S.; Pawar, N. B.; Mane, R. M.; Choudhury, S.; Hong, C. K.; Patil, P. S.; Patil, S. R.; Bhosale, P. N.; Kim, J. H., Microwave-assisted rapid synthesis of highly porous TiO2 thin films with nanocrystalline framework for efficient photoelectrochemical conversion. *Electrochimica Acta* (2014), *143*, 89-97./https://doi.org/10.1016/j.electacta.2014.07.149

Lal, S.; Razeeb, K. M.; Gautam, D., Enhanced Thermoelectric Properties of Electrodeposited Cu-Doped Te Films. *ACS Applied Energy Materials* (2020), *3* (4), 3262-3268./10.1021/acsaem.9b02153

Li, C.; Jiang, F.; Liu, C.; Wang, W.; Li, X.; Wang, T.; Xu, J., A simple thermoelectric device based on inorganic/organic composite thin film for energy harvesting. *Chemical Engineering Journal* (2017), *320*, 201-210./https://doi.org/10.1016/j.cej.2017.03.023

Li, C.; Sun, P.; Liu, C.; Xu, J.; Wang, T.; Wang, W.; Hou, J.; Jiang, F., Fabrication of flexible SWCNTs-Te composite films for improving thermoelectric properties. *Journal of Alloys and Compounds* (2017), *723*, 642-648./https://doi.org/10.1016/j.jallcom.2017.06.253

Li, G.; Garcia Fernandez, J.; Lara Ramos, D. A.; Barati, V.; Pérez, N.; Soldatov, I.; Reith, H.; Schierning, G.; Nielsch, K., Integrated microthermoelectric coolers with rapid response time and high device reliability. *Nature Electronics* (2018), *1* (10), 555-561./10.1038/s41928-018-0148-3

Li, H. H.; Zhang, P.; Liang, C. L.; Yang, J.; Zhou, M.; Lu, X. H.; Hope, G. A., Facile electrochemical synthesis of tellurium nanorods and their photoconductive properties. *Crystal Research and Technology* (2012), *47* (10), 1069-1074./10.1002/crat.201200273

Liang, Y.; Xiong, Y.; Zheng, J.; Xie, Z.; Chen, C.; Xu, L., Study of thermoelectric properties in the PEDOT:PSS/Te double-layer thin film devices. *Composites Communications* (2021), *27*, 100888./https://doi.org/10.1016/j.coco.2021.100888

Lim, S.-K.; Kim, M.-Y.; Oh, T.-S., Thermoelectric properties of the bismuth–antimony–telluride and the antimony–telluride films processed by electrodeposition for micro-device applications. *Thin Solid Films* (2009), *517* (14), 4199-4203./10.1016/j.tsf.2009.02.005

Liu, E.; Negm, A.; Howlader, M. M. R., Thermoelectric generation via tellurene for wearable applications: recent advances, research challenges, and future perspectives. *Materials Today Energy* (2021), *20*, 100625./https://doi.org/10.1016/j.mtener.2020.100625

Liu, Y.; Liu, P.; Jiang, Q.; Jiang, F.; Liu, J.; Liu, G.; Liu, C.; Du, Y.; Xu, J., Organic/inorganic hybrid for flexible thermoelectric fibers. *Chemical Engineering Journal* (2021), *405*, 126510./https://doi.org/10.1016/j.cej.2020.126510

Liu, Y.; Wang, W.; Liu, C.; Liu, C.; Xu, J.; Zhu, Z.; Yang, J.; Wang, Y.; Jiang, F., Effects of inorganic salt NaNbO3 composite on the thermoelectric properties of tellurium nanorods thin slice. *Journal of Alloys and Compounds* (2020), *849*, 156630./https://doi.org/10.1016/j.jallcom.2020.156630

Manikandan, M.; Dhanuskodi, S.; Maheswari, N.; Muralidharan, G.; Revathi, C.; Rajendra Kumar, R. T.; Mohan Rao, G., High performance supercapacitor and non-enzymatic hydrogen peroxide sensor based on tellurium nanoparticles. *Sensing and Bio-Sensing Research* (2017), *13*, 40-48./https://doi.org/10.1016/j.sbsr.2017.02.001

Manoharan, S.; Krishnamoorthy, K.; Mariappan, V. K.; Kesavan, D.; Kim, S.-J., Electrochemical deposition of vertically aligned tellurium nanorods on flexible carbon cloth for wearable supercapacitors. *Chemical Engineering Journal* (2021), *421*, 129548./https://doi.org/10.1016/j.cej.2021.129548

Meng, Q.; Cai, K.; Du, Y.; Chen, L., Preparation and thermoelectric properties of SWCNT/PEDOT:PSS coated tellurium nanorod composite films. *Journal of Alloys and Compounds* (2019), *778*, 163-169./https://doi.org/10.1016/j.jallcom.2018.10.381

Mohsen Momeni, M.; Najafi, M., Structural, morphological, optical and photoelectrochemical properties of ZnFe2O4 thin films grown via an electrodeposition method. *Inorganic Chemistry Communications* (2021), *132*, 108809./https://doi.org/10.1016/j.inoche.2021.108809

Mu, Y.; Gao, X.; Zhou, X.; Wang, H.; Lv, P.; Qiu, M.; Zhang, X., One-step synthesis and photoelectrical performance of feather-like tellurium on nickel foil. *Journal of Alloys and Compounds* (2018), *765*, 977-982./https://doi.org/10.1016/j.jallcom.2018.06.301

Newbrook, D. W.; Richards, S. P.; Greenacre, V. K.; Hector, A. L.; Levason, W.; Reid, G.; de Groot, C. H.; Huang, R., Improved thermoelectric performance of Bi2Se3 alloyed Bi2Te3 thin films via low pressure chemical vapour deposition. *Journal of Alloys and Compounds* (2020), *848*, 156523./https://doi.org/10.1016/j.jallcom.2020.156523

Ni, D.; Song, H.; Chen, Y.; Cai, K., Significantly enhanced thermoelectric performance of flexible PEDOT nanowire film via coating Te nanostructures. *Journal of Materiomics* (2020), *6* (2), 364-370./https://doi.org/10.1016/j.jmat.2019.07.001

Rheem, Y.; Chang, C. H.; Hangarter, C. M.; Park, D.-Y.; Lee, K.-H.; Jeong, Y.-S.; Myung, N. V., Synthesis of tellurium nanotubes by galvanic displacement. *Electrochimica Acta* (2010), *55* (7), 2472-2476./https://doi.org/10.1016/j.electacta.2009.12.002

Sabran, N. S.; Fadzallah, I. A.; Ono, T.; Said, S. M.; Sabri, M. F. M., Preparation and Characterization of Electrochemical Deposition Cobalt Triantimonide (CoSb3) Thick Film: Effects of Polyvinyl Alcohol (PVA) as an Additive. *Journal of Electronic Materials* (2019), *48* (8), 5003-5011./10.1007/s11664-019-07295-3

Saxena, M.; Bera, A. K.; Venkatesh, R., Wet chemical assisted synthesis of self assembled tellurium nanostructures with enhanced stability. *Materials Letters* (2021), *301*, 130300./https://doi.org/10.1016/j.matlet.2021.130300

Schoenleber, J.; Stein, N.; Boulanger, C., Influence of tartaric acid on diffusion coefficients of BiIII, SbIII, TeIV in aqueous medium: Application of electrodeposition of thermoelectric films. *Journal of Electroanalytical Chemistry* (2014), *724*, 111-117./10.1016/j.jelechem.2014.04.004

Schumacher, C.; Reinsberg, K. G.; Akinsinde, L.; Zastrow, S.; Heiderich, S.; Toellner, W.; Rampelberg, G.; Detavernier, C.; Broekaert, J. A. C.; Nielsch, K.; Bachmann, J., Optimization of Electrodeposited p-Doped Sb2Te3 Thermoelectric Films by Millisecond Potentiostatic Pulses. *Advanced Energy Materials* (2012), *2* (3), 345-352./10.1002/aenm.201100585

Schumacher, C.; Reinsberg, K. G.; Rostek, R.; Akinsinde, L.; Baessler, S.; Zastrow, S.; Rampelberg, G.; Woias, P.; Detavernier, C.; Broekaert, J. A. C.; Bachmann, J.; Nielsch, K., Optimizations of Pulsed Plated p and n-type Bi2Te3-Based Ternary Compounds by Annealing in Different Ambient Atmospheres. *Advanced Energy Materials* (2013), *3* (1), 95-104./10.1002/aenm.201200417

Shen, J.; Jia, S.; Shi, N.; Ge, Q.; Gotoh, T.; Lv, S.; Liu, Q.; Dronskowski, R.; Elliott, S. R.; Song, Z.; Zhu, M., Elemental electrical switch enabling phase segregation–free operation. *Science* (2021), *374* (6573), 1390-1394./10.1126/science.abi6332

Shen, Y.; Yan, X.; Zhao, S.; Chen, X.; Wei, D.; Gao, S.; Han, C.; Meng, D., Ethanol sensing properties of TeO2 thin films prepared by non-hydrolytic sol–gel process. *Sensors and Actuators B: Chemical* (2016), *230*, 667-672./https://doi.org/10.1016/j.snb.2016.02.118

Song, H.; Cai, K., Preparation and properties of PEDOT:PSS/Te nanorod composite films for flexible thermoelectric power generator. *Energy* (2017), *125*, 519-525./https://doi.org/10.1016/j.energy.2017.01.037

Sudarshan, C.; Jayakumar, S.; Vaideki, K.; Sudakar, C., Te-rich Bi2Te3 thin films by electron−beam deposition: Structural, electrical, optical and thermoelectric properties. *Thin Solid Films* (2020), *713*, 138355./https://doi.org/10.1016/j.tsf.2020.138355

Sugahara, T.; Ekubaru, Y.; Nong, N. V.; Kagami, N.; Ohata, K.; Hung, L. T.; Okajima, M.; Nambu, S.; Suganuma, K., Fabrication with Semiconductor Packaging Technologies and Characterization of a Large-Scale Flexible Thermoelectric Module. *Advanced Materials Technologies* (2019), *4* (2), 1800556./https://doi.org/10.1002/admt.201800556

Tang, L.; Tan, J.; Nong, H.; Liu, B.; Cheng, H.-M., Chemical Vapor Deposition Growth of Two-Dimensional Compound Materials: Controllability, Material Quality, and Growth Mechanism. *Accounts of Materials Research* (2021), *2* (1), 36-47./10.1021/accountsmr.0c00063

Tishkevich, D. I.; Grabchikov, S. S.; Tsybulskaya, L. S.; Shendyukov, V. S.; Perevoznikov, S. S.;

Trukhanov, S. V.; Trukhanova, E. L.; Trukhanov, A. V.; Vinnik, D. A., Electrochemical deposition regimes and critical influence of organic additives on the structure of Bi films. *Journal of Alloys and Compounds* (2018), *735*, 1943-1948./https://doi.org/10.1016/j.jallcom.2017.11.329

Tsao, Y.-H.; Husain, R. A.; Lin, Y.-J.; Khan, I.; Chen, S.-W.; Lin, Z.-H., A self-powered mercury ion nanosensor based on the thermoelectric effect and chemical transformation mechanism. *Nano Energy* (2019), *62*, 268-274./https://doi.org/10.1016/j.nanoen.2019.05.032

Tsiulyanu, D.; Mocreac, O., Concentration induced damping of gas sensitivity in ultrathin tellurium films. *Sensors and Actuators B: Chemical* (2013), *177*, 1128-1133./https://doi.org/10.1016/j.snb.2012.12.022

Vale, S.; Heber, L.; Coelho, P. J.; Silva, C. M., Parametric study of a thermoelectric generator system for exhaust gas energy recovery in diesel road freight transportation. *Energy Conversion and Management* (2017), *133*, 167-177./https://doi.org/10.1016/j.enconman.2016.11.064

Van Toan, N.; Tuoi, T. T. K.; Ono, T., Thermoelectric generators for heat harvesting: From material synthesis to device fabrication. *Energy Conversion and Management* (2020), *225*, 113442./https://doi.org/10.1016/j.enconman.2020.113442

Vanalakar, S. A.; Galal, A.; Singh, V. N.; Min, H., A review of nanostructured thin films for gas sensing and corrosion protection. *Mediterranean Journal of Chemistry* (2018), *7*, 433-451

Waldiya, M.; Bhagat, D.; R, N.; Singh, S.; Kumar, A.; Ray, A.; Mukhopadhyay, I., Development of highly sensitive H2O2 redox sensor from electrodeposited tellurium nanoparticles using ionic liquid. *Biosensors and Bioelectronics* (2019), *132*, 319-325./https://doi.org/10.1016/j.bios.2019.02.050

Wang, S.; Wen, H.; Guan, W.; Zhang, L.; Ma, D.; Huang, S.; Wang, J., Fabricating two-dimensional nanostructured tellurium thin films via pyrolyzing a single-source molecular precursor. *Thin Solid Films* (2010), *518* (15), 4215-4220./https://doi.org/10.1016/j.tsf.2009.12.081

Wang, W.; Li, C.; Li, X.; Jia, Y.; Jiang, F.; Liu, C.; Tan, R.; Xu, J., Fabrication of freestanding tellurium nanofilm and its thermoelectric performance. *Thin Solid Films* (2018), *654*, 23-29./https://doi.org/10.1016/j.tsf.2018.03.073

Wang, Y.; Zhu, W.; Deng, Y.; Zhu, P.; Yu, Y.; Hu, S.; Zhang, R., High-sensitivity self-powered temperature/pressure sensor based on flexible Bi-Te thermoelectric film and porous microconed elastomer. *Journal of Materials Science & Technology* (2022), *103*, 1-7./https://doi.org/10.1016/j.jmst.2021.07.008

Wu, T.; Zhang, M.; Lee, K.-H.; Kim, S.-i.; Choa, Y.; Myung, N. V., Synthesis of Tellurium Heterostructures by Galvanic Displacement Reaction of Zinc in Alkaline Baths. *Electrochimica Acta* (2014), *150*, 298-307./https://doi.org/10.1016/j.electacta.2014.10.099

Yang, H.-N.; He, S.-J.; Zhang, T.; Man, J.-X.; Zhao, Y.; Jiang, N.; Wang, D.-K.; Lu, Z.-H., Molecular orientation and thermal stability of thin-film organic semiconductors. *Organic Electronics* (2021), *88*, 106014./https://doi.org/10.1016/j.orgel.2020.106014

Yang, J.; Jia, Y.; Liu, Y.; Liu, P.; Wang, Y.; Li, M.; Jiang, F.; Lan, X.; Xu, J., PEDOT:PSS/PVA/Te ternary composite fibers toward flexible thermoelectric generator. *Composites Communications* (2021), *27*, 100855./https://doi.org/10.1016/j.coco.2021.100855

Yuan, Z.; Zhao, Q.; Xie, C.; Liang, J.; Duan, X.; Duan, Z.; Li, S.; Jiang, Y.; Tai, H., Gold-loaded tellurium nanobelts gas sensor for ppt-level NO2 detection at room temperature. *Sensors and Actuators B: Chemical* (2022), *355*, 131300./https://doi.org/10.1016/j.snb.2021.131300

Zhao, X.; Shi, J.; Yin, Q.; Dong, Z.; Zhang, Y.; Kang, L.; Yu, Q.; Chen, C.; Li, J.; Liu, X.; Zhang, K., Controllable synthesis of high-quality two-dimensional tellurium by a facile chemical vapor transport strategy. *iScience* (2022), *25* (1), 103594./https://doi.org/10.1016/j.isci.2021.103594

Zheng, Z.-h.; Fan, P.; Luo, J.-t.; Cai, X.-m.; Liang, G.-x.; Zhang, D.-p.; Ye, F., Thermoelectric properties of bismuth antimony tellurium thin films through bilayer annealing prepared by ion beam sputtering deposition. *Thin Solid Films* (2014), *562*, 181-184./https://doi.org/10.1016/j.tsf.2014.04.043